Diplomarbeit

Investigation of the role of micro-RNA 451 in traumatic brain injury-induced neurogenesis

An experimental study in controlled cortical impact model of mice

eingereicht von

Benjamin Daniel Klaus

zur Erlangung des akademischen Grades

Doktor der gesamten Heilkunde

(Dr. med. univ.)

an der

Medizinischen Universität Graz

ausgeführt an der

Klinik für Neurochirurgie

Forschungseinheit für Experimentelle Neurotraumatologie

unter der Anleitung von

Univ. Prof.in Dr.in rer nat. Ute Schäfer und Muammer Üçal, PhD

Graz, 03.09.2019

STATUTORY DECLARATION

Ich erkläre ehrenwörtlich, dass ich die vorliegende Arbeit selbstständig und ohne fremde Hilfe verfasst habe, andere als die angegebenen Quellen nicht verwendet habe und die den benutzten Quellen wörtlich oder inhaltlich entnommenen Stellen als solche kenntlich gemacht habe.

Graz, am 03.09.2019 **Benjamin Klaus eh.**

ACKNOWLEDGEMENTS

I would like to thank my supervisor Professor Dr. Ute Schäfer for providing this fascinating topic and for agreeing to supervise my diploma thesis.

I would like to express my innermost gratitude to Muammer Üçal, PhD. Without him this work probably would not exist. He introduced me into this scientific field and guided me through the whole development process of this diploma thesis with incomparable patience and expertise. He has substantially contributed to my skills and the problem-solving approaches I could learn from him will help me in whichever field of medicine I will find myself in the future.

My special thanks got to the members of the Research Unit of Experimental Neurotraumatology, Priv.-Doz. Dr. Silke Patz, Vanessa Mair, MSc, BMA Gerda Grünbacher, Sriveena Srinivasaiah, MSc, Mag. Ulrike Zefferer, not only for their assistance but also for the warm welcome in their extraordinary team.

I owe my deepest gratitude to my great friend Nikolaus Kopp, BSc for the motivating discussions and especially his help with a Python script, which facilitates data analyses in this diploma thesis.

Finally, my special thanks go to my parents Werner and Susanne, for their omnipresent and loving support during my studies, my sister Katharina for optimizing my English skills during the process of writing and to Gloria, whose generous support and encouragement helped me to find an efficient work-life-balance.

TABLE OF CONTENTS

ABBREVIATIONS and DEFINITIONS

AL	Avoidance learning
AMPK	AMP-activated protein kinase
BrdU	Bromodeoxyuridine
CCI	Controlled cortical impact
DAPI	4′,6-Diamidin-2-phenylindol
FA	Formaldehyde
FPI	Fluid percussion injury
ICP	intracerebral pressure
ip	intraperitoneal
ko	knock-out
LKB1	liver kinase B 1
miR	micro-RNA
miR451	micro-RNA 451
miR451$^{-/-}$	micro-RNA 451 knock-out
modCCI	moderate controlled cortical impact
NeuN	neuronal nuclei protein, RNA binding fox-1 homolog 3
NMDA	N-Methyl-D-Aspartate
NPC	neural precursor cell
NSAID	nonsteroidal anti-inflammatory drug
NSC	neural stem cell
nt	nucleotide
PBS	phosphate buffered saline
PL	Place learning
revPL	reversed Place learning
sc	subcutaneous
SGZ	subgranular zone
SVZ	subventricular zone
TBI	Traumatic brain injury
VEGF	vascular endothelial growth factor
wt	wild-type

LIST OF FIGURES

LIST OF TABLES

ZUSAMMENFASSUNG

Ziel: Das Ziel dieser Studie ist es, die potentielle Rolle der micro-RNA 451 in der trauma-assoziierten Neurogenese aufzuzeigen, indem das Lernverhalten und histologische Veränderungen in „wild-type“ und micro-RNA 451 knock-out Mäusen nach einem Schädel-Hirn-Trauma analysiert werden.

Einleitung: Die Rolle von micro-RNAs; kleinen, endogenen, nicht-codierenden, RNA-Molekülen, gelangt mehr und mehr in den Fokus von Studien. Eine dieser micro-RNAs ist die micro-RNA 451, deren Einfluss auf die Tumorgenese, besonders in der Entwicklung des Glioblastoma multiforme beschrieben wurde. Auch ein Zusammenhang dieser micro-RNA 451 mit Schädelhirntraumata wurde beobachtet, indem eine erhöhte Konzentration von micro-RNA 451 im Liquor von Schädelhirntrauma-Patienten gemessen wurde. Auch der konkrete Einfluss der micro-RNA 451 auf den Differenzierungsprozess von Neuronen konnte *in-vitro* gezeigt.

Methoden: „Wild-type“ und micro-RNA 451 knock-out Mäuse wurden kraniektomiert und es wurde ein mittelschweres kortikales Trauma im Bereich des rechten Hippocampus appliziert. Neu proliferierte Zellen wurden mit intraperitonealen BrdU-Injektionen (vom 2. bis 8. postoperativen Tag) markiert. Mögliche Unterschiede in der Gedächtnisbildung und dem räumlichen Lernen wurden mit einer Verhaltenstestung im IntelliCage überwacht und analysiert. Die erfolgreiche Differenzierung in reife Neuronen wurde durch die immunhistochemische Färbung von BrdU und NeuN 45 Tage nach dem Trauma beurteilt.

Ergebnisse: Die Zunahme der Neurogenese im Gyrus dentatus des Hippocampus 45 Tage nach dem Trauma war in den micro-RNA 451 knock-out Mäusen deutlicher erkennbar, sowohl ipsilateral als auch contralateral. Im Hilus wurde in beiden Gruppen eine erhöhte Zahl neugebildeter Neurone beobachtet, dieser Effekt war in den micro-RNA 451 knock-out Mäusen stärker erkennbar. Es wurde eine traumabedingte Verschlechterung des Kurzzeitgedächtnis im IntelliCage beobachtet, jedoch war diese Verschlechterung war unabhängig von der micro-RNA 451. Posttraumatische Defizite im Lernverhalten konnten in diesem IntelliCage Test set-up weder in den „wild-type“, noch in den micro-RNA 451 knock-out Mäusen gezeigt werden.

Diskussion: Die histologischen Ergebnisse deuten darauf hin, dass die micro-RNA 451 eine wichtige Rolle in der Neurogenese nach einem Schädelhirntrauma spielen könnte. Diese gesteigerte Neurogenese am 45. Tag nach dem Schädelhirntrauma zeigt jedoch keine Korrelationen in der vom 16. - 20. Tag durchgeführten Verhaltenstestung. Die erhöhte Anzahl an neugebildeten Neuronen, welche untypischer Weise von der subgranular Zone des Hippocampus in den Hilus migriert sind suggeriert, dass die micro-RNA 451 knock-out Mäuse ein erhöhtes Potenzial für die Entwicklung einer posttraumatischen Epilepsie aufweisen. Ob diese ungewöhnliche Migration von Neuronen aus der SGZ in den Hilus des Hippocampus nur durch eine erhöhte Proliferation zu erklären ist, oder die micro-RNA 451 eine regulatorische Rolle in der neuronalen Migration hat, sollte weiterhin untersucht werden.

ABSTRACT

Aim: The aim of this study is to evaluate the potential role of miR451 in injury-induced neurogenesis by comparing behavioural and histological differences in miR451$^{-/-}$ and wild-type mice in an in-vivo trauma model.

Introduction: The role of micro-RNAs, which are endogenous, non-coding, small RNA molecules, in the posttranscriptional regulation of gene expression has more and more come into focus. One of these micro-RNAs is the miR451, whose impact on oncogenesis, especially in the glioblastoma multiforme has been described and which might also influence the endogenous response to injury-induced loss of neuronal tissue. MiR451 is increased in the cerebrospinal fluid of patients with traumatic brain injury compared to non-injured controls and the influence of miR451 in neurogenic maturation processes has been shown *in vitro*.

Methods: Wild-type mice and miR451$^{-/-}$ mice were craniectomized, and received a moderate brain trauma with controlled cortical impact (CCI). Newly proliferating cells were labelled with BrdU injections after CCI (at days 2-8). Potential differences in memory formation and spatial learning were monitored with a behavioural testing setup in an IntelliCage. Post-CCI neurogenesis was assessed with BrdU/NeuN co-immunostaining.

Results: Increase in neurogenesis at the hippocampal dentate gyri detected 45 days after CCI was more prominent in the miR451$^{-/-}$ animals, both at the ipsi- and the contralateral sides. Newly produced neurons were detected in the hilus after brain injury in both animal groups, but the increase was particularly pronounced in the miR451$^{-/-}$ animals. A CCI-induced disturbance in short-term memory was detected in the IntelliCage, but the effect was independent of miR451 expression. CCI-induced deficits in the learning performance in IntelliCage were not detected in wild-type or miR451$^{-/-}$ mice.

Discussion: Histological findings suggest that miR451$^{-/-}$ could play an important role in post-TBI neurogenesis. However, the higher neurogenesis in the dentate gyrus at day 45 did not show any detectable correlation in functional behavioural tests at 16-20 days post-TBI. Increased number of newly produced neurons aberrantly migrated from SGZ to hilus suggests that miR451$^{-/-}$ animals could be more susceptible to TBI-induced epileptogenesis. Whether this aberrant migration is caused purely by higher proliferation or whether miR451 has a regulatory role in neuronal migration remain to be further elucidated.

1 INTRODUCTION

1.1 Traumatic Brain Injury

Traumatic brain injury (TBI) is a leading cause of death and disability among the young adults. Consequences ranging from post-TBI stress disorders to severe disabilities create a huge burden on the life quality of not only the patients but also for the family members that have to spend several years with patient care. Loss of productive years and high patient care costs, on the other hand, create a serious socioeconomic burden for the society and the public health. The Centres for Disease Control and Prevention of the United States reported that around 1.7 million individuals suffered a TBI each year from 2002 to 2006 only in the United States. With an estimated incidence rate of 538/100.000, TBI is responsible for almost a third (30.5%) of fatal injuries in the US (1,2).

In Austria TBI has an incidence rate of 303/100.000 per year and a mortality rate of 11/100.000, which are comparable to other European countries(3). The number of TBIs peaks within two groups; male teens and female octogenarians, representing very different TBI aetiologies. The main causes for the high number of geriatric patients are falls, while the TBIs in young male individuals are mostly accident-related(3).

A traumatic brain injury is characterized by a trauma-related loss of neuronal tissue. Due to the complexity of the aetiologies and the pathophysiological processes which lead to loss of cerebral tissue, further classification in TBIs is essential. The variety of aetiologies cannot be classified properly only by severity, because the localisation, the expansion, the injury mechanism and the intactness of the skull also play crucial roles in the pathophysiology of TBI.

Concerning the intactness of the skull, TBIs are classified into two groups; open and closed TBI. Also, the localisation of the impact and the functional correlates of the affected anatomical regions have a great influence on the development of the injury. The injury mechanism of TBI depends on the way mechanical forces work on the tissue, ranging from direct impact (penetrating) to non-contact (concussive or shearing)(4). The mechanical aetiology of TBI influences the expansion of the trauma. A focal TBI limited to a regional loss of brain tissue is more likely seen in penetrating injuries, while a diffuse injury is more often observed in concussions.

The actual brain damage can be classified in primary and secondary damage (*Figure 1*). Primary damage describes the actual impact on the head and the immediate loss of tissue. The secondary damage results from the pathophysiological consequences such as oedema, hemorrhage, hypo-/hyper-perfusion, inflammation and incarceration of cerebellar or cerebral structures caused by an increase of the cerebral pressure.

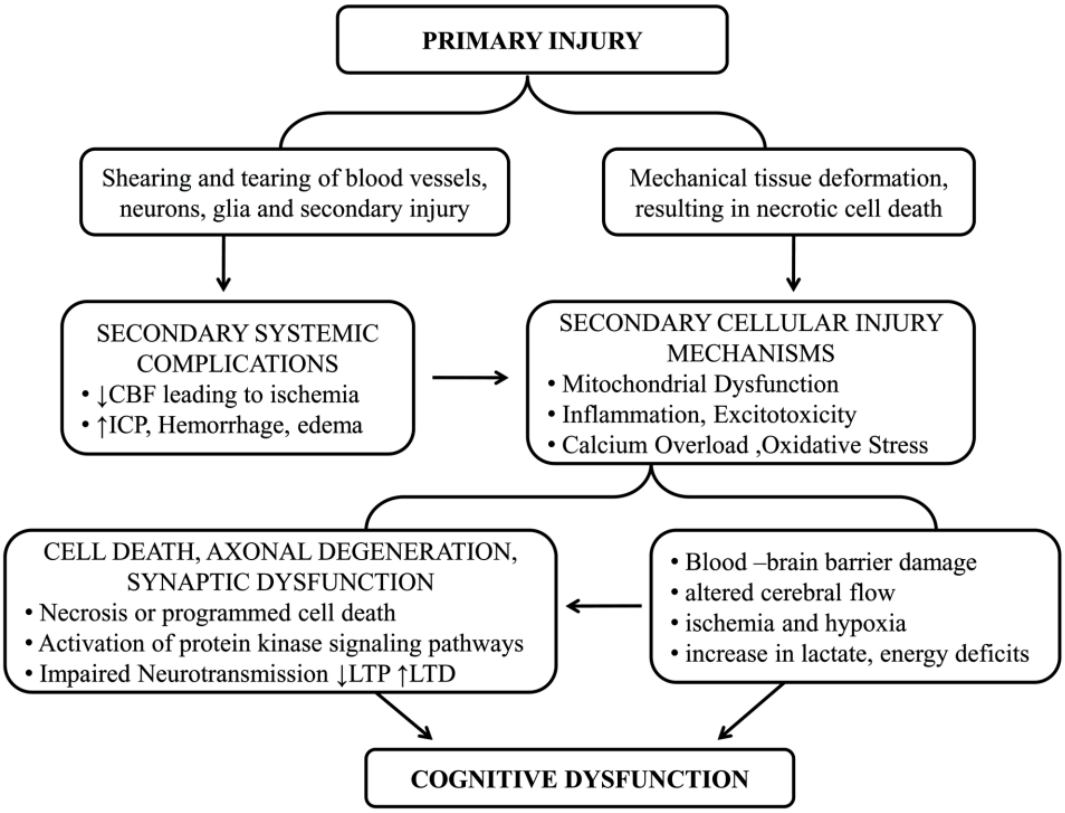

Figure 1: Overview of primary and secondary damages in TBI

The pathophysiological development of TBI is a complex process involving various interacting factors and mechanisms. The primary injury is characterised by shearing, tearing or mechanical tissue deformation resulting in an immediate necrosis of neuronal tissue. The secondary injury arises out of the primary damage and can range from systemic complications (reactive systemic hypertension due to increased intracerebral pressure) to cellular injury mechanisms as mitochondrial dysfunction, excitotoxicity or inflammation. The figure was adapted from Kaur and Sharma, 2017 (5).

While the primary physical damage can only be avoided by preventive measures, post-TBI treatment strategies solely depend on the attenuation of the secondary damage to prevent deepening insult in the brain tissue. Accordingly, several years of clinical and experimental research has been conducted to understand the TBI

pathophysiology in order to clinically target one or more secondary damage mechanisms with a wish to improve prognosis as well as to reduce the mortality, the lesion size and the severity of disability afterwards (5–9)
Given the limited regenerative capacity of nervous tissue, therapeutic approaches after a TBI are largely dependent on rehabilitation. Modulation of endogenous neurogenesis, therefore, comprises another major field to enhance repair and regeneration after a TBI. On that account, the necessity of understanding the factors and processes, which modulate endogenous neurogenesis in adult brain emerges to be critical for regenerative and restorative treatments after a TBI.

1.2 Animal model

In order to understand the impact of traumatic brain injuries (TBIs) on adult neurogenesis, various animal models have been established and used in different studies. Controlled cortical impact (CCI), fluid percussion injury (FPI), weight drop models, the penetrating ballistic-like brain injury and the blast brain injury are some of the frequently used experimental TBI models. Each of these models have been developed to answer questions related to the different aspects of the head trauma (diffuse or focal, penetrating or closed head trauma) and show differences in representation of post-TBI sequelae (intracranial pressure increase, *contrecoup* injury, haemorrhage, diffuse axonal damage) and hampering the comparability of them altogether. Accordingly, studies using different models have shown inconsistencies in their results with respect to the changes in neurogenesis in subventricular zone (SVZ) and subgranular zone (SGZ) of hippocampus after TBI (10–14).
Trauma-induced neurogenesis was consistently shown in CCI (9,11,12,14–17) allowing it to be used as an appropriate model to study molecular mechanisms influencing injury-induced neurogenesis. The characteristics of a controlled cortical impact trauma model are focal damage, produced by a piston which strikes the exposed surface of the brain with a predefined velocity, depth and diameter (*Figure 2*). A craniectomy is necessary to expose the surface of the brain in order to produce a focal trauma. This model has a great variety of adaptations not only in trauma severity (depth of penetration) but also in localisation, speed of penetration and dwelling time of the piston in the brain tissue during the impact. The CCI trauma model is representing a primary damaging controlled penetrating

trauma with direct axonal damage, focal bleeding and laceration of the meninges at the impact site (18).

Secondary damages caused by a CCI range from an increase of cerebral pressure to secondary bleeding and infarction due to ruptured blood vessels. The severity of these traumata can be controlled mainly by the diameter of the piston, the localisation and the depth of impact in the brain. Therefore, the CCI is a well established, adaptable trauma model, which represents various aspects of TBI (18).

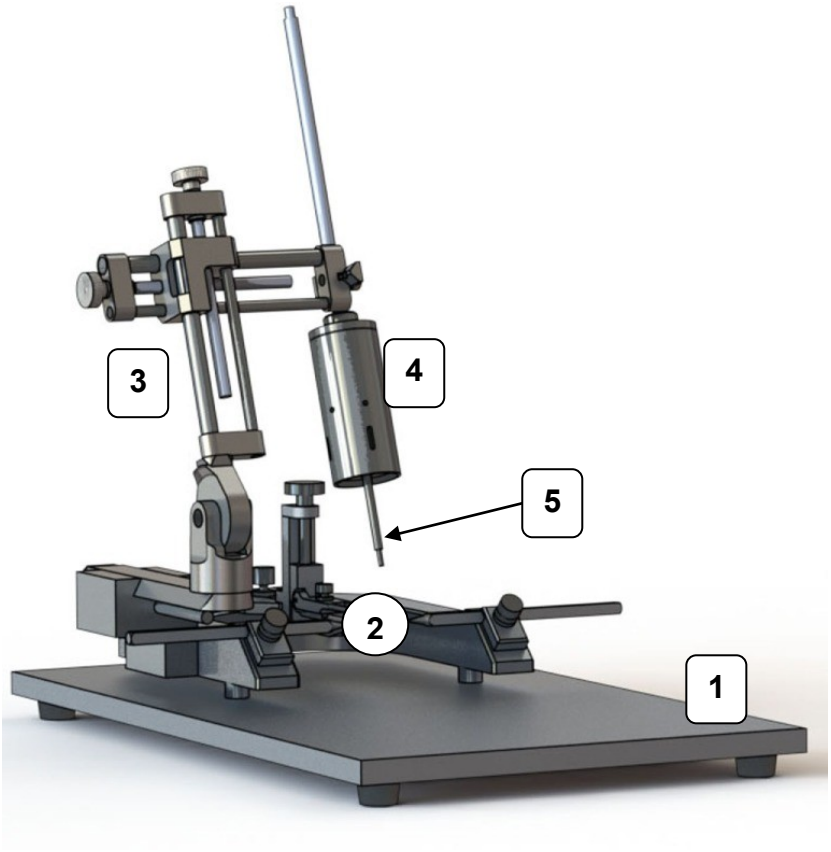

Figure 2: Schematic view of a CCI-Setup

*The CCI-Setup used in this study consists of a stereotactic frame (**1**), which allows the stable and precise positioning of the animals head (**2**), as well as the stereotactic arm (**3**) with the electromagnetic CCI-device (**4**). The piston tip (**5**), penetrating the brain, can be exchanged to have different diameters of the resulting lesion. The picture was adapted from Osier and Dixon 2016,* (19)*.*

1.3 Adult Neurogenesis

Contrary to the long-held perception of neurogenesis as a purely prenatal process, recent studies shifted the focus to adult neurogenesis. In 1962 Joseph Altman

raised the hypothesis of the formation of newly born neurons in adult brains of mammals (20). 1965 Joseph Altman published “Autoradiographic and histological evidence of postnatal hippocampal neurogenesis in rats” (21). Although this field of neuroscience almost sank into oblivion in the 1970s and 1980s, Eriksson et al. initiated great interest in reprocessing adult neurogenesis, when he described adult neurogenesis in human brains in 1998 (22). Since then, adult neurogenesis has become one of the hottest research topics in neuroscience (23).

Adult neurogenesis is defined as the proliferation and differentiation of neural stem cells (NSCs) and neural progenitor cells (NPCs) in restricted areas in the adult mammalian brain. These NSCs and NPCs are precursor cells for all types of neurons, neural cells and glial cells (24).

The symmetric division of NSCs in the neurogenic regions provides a pool of multipotent cells, which can differentiate and maturate become either neuroblasts or glioblasts (*Figure 3*). While the major proportion of NPCs develop into glioblasts that differentiate to produce astrocytes and oligodendrocytes, a small proportion of them find their way into neuroblasts, which differentiate into the neurons.

There are two main localisations for neurogenesis in the physiological mammalian brain described; the subventricular zone (SVZ) of the lateral ventricles and the subgranular zone (SGZ) of the dentate gyrus (22,25,26) (*Figure 4*).

New neurons produced in the SVZ migrate through the rostral migratory stream to the olfactory bulb, where they differentiate into granule and periglomerular interneurons (26,27).

In the SGZ of the hippocampal dentate gyrus, new dentate granule cells are produced and migrate into the granular cell layer where the development of dendrites and axons towards CA3 leads to the integration into the existing neural network as new mature granule cells. Some of the progenitor cells differentiate into astrocytes or radial glia-like cells (7,8).

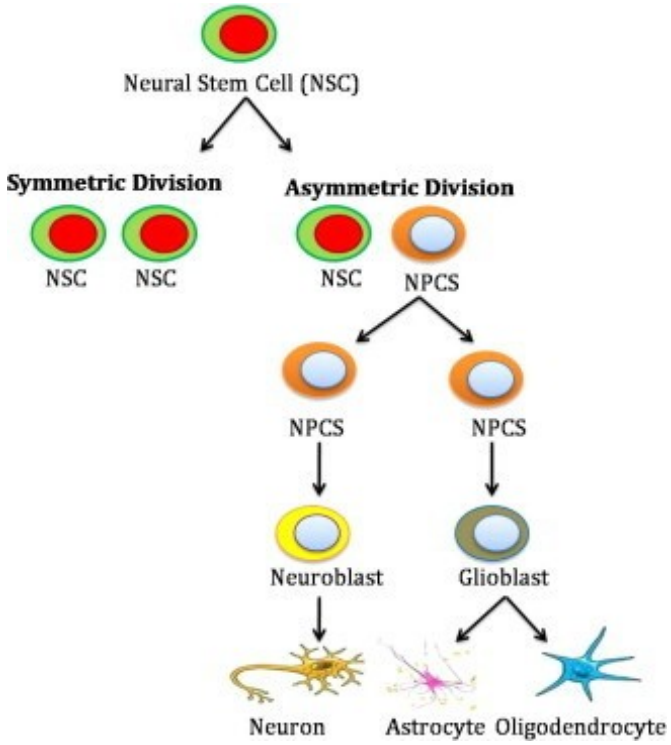

Figure 3: Overview of self-renewal and differentiation of neural stem cells.
The neural stem cells (NSCs) in the neurogenic regions fulfil two major tasks. Proliferation by symmetric division to keep the pool of NSCs and asymmetric division as start of the differentiation process. During differentiation, NSCs evolve into neural progenitor cells, which differentiate either in neuroblasts and mature neurons, or into glioblasts and astrocytes or oligodendrocytes. The figure was adapted from Vishwakarma et al., 2019 (30)

Adult neurogenesis in the subgranular zone of the hippocampal dentate gyrus is considered to functionally influence the hippocampal plasticity. The integration of these newly produced neurons in the existing neuronal network of hippocampus lasts for around 7 weeks (23). Proliferation, differentiation, migration and integration of these newly born progenitor cells is regulated by various factors. These factors seem to be restricted to the so-called neurogenic “niche” in the subgranular zone.

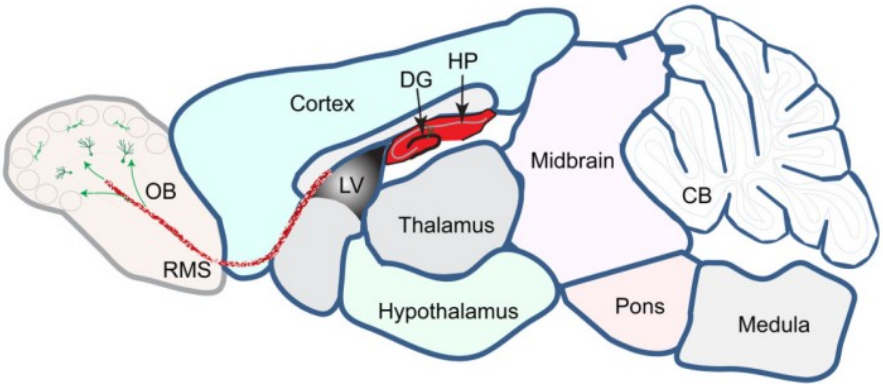

Figure 4: Overview of neurogenic regions in an adult rodent brain

Schematic sagittal view of a rodent brain, showing the dentate gyrus (DG) of hippocampus (HP) and the lateral ventricle with its subventricular zone as two main localisations for adult neurogenesis.

Cells proliferated in the subventricular zone migrate through the rostral migratory stream (RMS) into the olfactory bulb (OB), where they maturate into granule cells and periglomerular neurons. The figure was adapted from Ming and Song, 2011 (26).

In addition to NPCs and NSCs, various immune cells, endothelial cells, glial cells and immature neurons can be found in this very complex environment. The dynamicity and potential of this so called neurogenic niche is also characterised by its extracellular matrix and various humoral regulating factors (e.g. VEGF), which enable the development of neurons (31).

Under these very special conditions, the process of adult neurogenesis takes place in four phases: The precursor cell phase, the early survival phase, the post-mitotic maturation phase and the late survival phase (32,33).

In the ***precursor cell phase*** radial glia-like stem cells, which proliferate continuously to keep a reservoir of precursor cells for neurogenic differentiation, leave the mitotic cell cycle. In the following ***early survival phase*** most of these newborn cells go under apoptosis. The remaining cells enter the ***post-mitotic maturation phase***, where the formation of functionally active connections starts. During the post-mitotic maturation phase, integration via the development of dendrites and axons into the surrounding neural network occurs. After the expression of synaptic connections, the last state of the newborn neurons, the ***late survival phase***, is reached. The late survival phase is far from a steady state of the new neurons, it is the optimisation of the integrity in the existing neural network(33).

The regulation of adult neurogenesis, especially in the hippocampus, is closely linked to hippocampal tasks and activity. A higher activity level of the hippocampus leads to functionally better integrated new neurons, which in turn is thought to result in higher hippocampal plasticity leading to a better performance in hippocampus related tasks, such as episodic and spatial memory (34).
Besides the investigation of inductive and regulatory mechanisms in these two neurogenic regions under physiological conditions, the potential impact of pathophysiological changes as seen in ischemia, inflammation, or trauma came into focus. The adult neurogenesis seems to be induced as a response to injury, ischemia or inflammation associated loss of neurons (35), possibly as an endogenous repair attempt. Following a TBI, increased proliferation of NSCs and NPCs have been documented by several groups (10,36), but whether and how this enhanced proliferation contributes to the recovery after a TBI, remained controversial, as it was not always correlated to a functional improvement (15).

1.4 MicroRNAs in neurogenesis

In 1993, while investigating the role of the lin 4 gene, Lee et al. discovered an important player in the post-transcriptional regulation of gene expression, namely small non-coding RNA particles, known as microRNAs (miRNAs) (37). These approximately 22 nucleotides long endogenous RNA molecules are by now seen as important regulators of tissue-specific cell behaviour. Their potential influence on the output of various protein-coding genes made them a target for different therapeutic approaches (38). Since then, more than 2500 different human miRNAs have been registered at the miRBase (www.miRBase.org) (39,40). As each influences the post-transcriptional processing of several target genes, this shows the immense impact of miRNAs on the regulation of gene expression.
The complex development of functional neurons in the brain is closely linked to the role of miRNAs (41) in fine-tuning cellular processes by interfering with mRNA in a post-transcriptional way (42,43). MiRNAs are able to regulate the process of neural development at all different stages of neurogenesis ranging from the proliferation and differentiation of NSCs and NPCs to the complex migration of newly born neurons up to the integration into the existing neuronal network (miR-9 (44),miR-123, (45), miR-125b, miR-132 (46), miR-137 (47), miR-138 (48), miR-184 (49), miR-195 (50), miR-451(51)). The great variety of possibilities where miRNAs

can regulate or modulate neurogenesis makes them a possible target for therapeutic or diagnostic approaches of different neurological diseases (52).
As most of the miRNAs, miR451 has different target genes leading to various observed impacts of miR451 up-regulation or down-regulation. MiR451 may have a promoting influence on erythroid differentiation and maturation (53) and also an impact on tumorigenesis. In non-small cell lung cancer tissue, a down-regulation of miR-451 expression compared to non-cancerous lung tissue was observed (54,55). Also in gastric cancer and osteosarcoma, down-regulation of miR-451 correlated with malignancy (56–58). The impact of miR451 down-regulation on the oncogenesis of glioblastoma multiforme has been shown in recent studies. MiR-451 is influencing the adaptability of glioma cells to metabolic stress by regulating the LKB1/AMPK pathway, leading to the homeostasis of proliferation and migration (59).
In a recent study by Research Unit of Experimental Neurotraumatology at the Medical University of Graz, miR-451 was shown to influence neurogenesis *in vitro* and *in vivo* (51). Ntera-2 cells, overexpressing miR451, showed an accelerated differentiation compared to transduced control cells, suggesting an influence of miR451 in neurogenesis. Preliminary data shows not any gross abnormalities in brain of miR451$^{-/-}$ animals, which indicates that the absence of miR451 has been compensated by other mechanisms. That allows the reflection, if the role of miR451 is restricted to a pathophysiological environment as in tumorigenesis or TBI. Indeed, in a previous study by the same group, miR451 was found to be exclusively enriched in the microparticles released into the cerebrospinal fluid (CSF) following TBI in clinical patients, compared to the non-injured control patients (*Figure 5*) (60).
These recent findings suggest a potential impact of miR-451 on neural differentiation and maturation of neuronal cells and a correlation in a TBI-like setting *in vivo*.

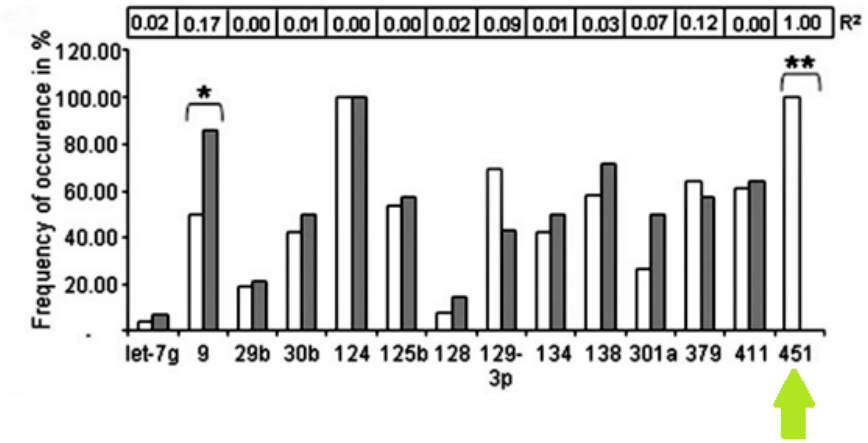

Figure 5: Presence of different miRNAs in the CSF of TBI patients.

CSF of TBI patients (white bars) compared to the CSF of healthy controls (grey bars). miR451 occurs exclusively in the CSF of TBI patients. The figure was adapted from Patz et al., 2013 (60).

1.4.1 Hypothesis:

Adult neurogenesis is known to be induced by TBI as a possible attempt for repair and recovery and a correlation of miR-451 and TBI has been shown in CSF analyses.

With respect to these recent findings of our group, we hypothesised that injury-induced neurogenesis in the dentate gyrus of hippocampus is regulated differentially in miR451$^{-/-}$ compared to wild-type mice.

In order to answer this question, a moderate CCI model was established, to have a comparable focal injury on the right parietal cortex.

The first aim of this study was to assess injury-induced neurogenesis by quantification of newly proliferated and differentiated neurons with co-immunostaining of BrdU and NeuN.

The second aim of this study was to find functional correlates to the differences in neurogenesis, by evaluating the behavioural and learning capabilities of miR451$^{-/-}$ and wild-type mice.

Revealing the exact role of miR-451 in injury-induced neurogenesis can uncover its therapeutic potential for promoting endogenous repair mechanisms after brain injuries.

2 MATERIAL and METHODS

2.1 Ethic statement, Animal Husbandry and Grouping

Care and use of animals were conducted in accordance with the ethical guidelines and all animal experiments were approved by the Bundesministerium für Wissenschaft, Forschung und Wirtschaft (Licence Number: BMWF-66.010/0099-II/3b/2013).

The animals were kept in standard conditions in groups of up to 5 animals per cage, with food and water *ad libitum*. The animals were held in a 12h:12h light-dark cycle in a controlled environment at the animal facility of Biomedical Research Institute in Medical University of Graz.

For the experiments, adult male mice were used with an average age of 13 ±1.5 weeks. On the day of the surgery, the animals had a mean weight of 25 g ± 1,24g. The miR451$^{-/-}$ mice were of *Aldha1* strain with the C57BL6 genetic background and they were obtained through in-house breedings at the facilities of Research Unit of Experimental Neurotraumatology (BMWF-66.010/0100-II/3b/2013). Adult male C57BL/6N mice were ordered from Charles River Laboratories and used as wild-type controls. Externally ordered animals were kept at least 1 week for habituation at the animal facility before the surgery.

2.2 Exclusion criteria:

Animals, which could not achieve a sufficient hydration during the behavioural testing in IntelliCage, were transferred to the conventional cages and excluded from further behavioural testing. These animals were also excluded from further histological analyses.

Animals which lost their RFID-Chip during the behavioural testing phases (PL, revPL and AL) in IntelliCage were excluded from further analysis.

2.3 Trauma model and surgery

2.3.1 Anaesthesia

To provide sufficient anaesthesia during surgery and trauma, an intraperitoneal injection with ketamine (100mg/ml, aniMedica GmbH, Germany) and xylazine (20mg/ml, Bayer Austria GmbH, Austria) was used. Xylazine is an -2-adrenergic

receptor agonist leading to sedation, analgesia and in a limited extent to muscle relaxation.

Ketamine as an NMDA (N-Methyl-D-Aspartate) receptor antagonist inhibits the NMDA-dependent release of acetylcholine and inhibits the glutamate receptors leading to a hypnotic and analgesic effect. But ketamine also inhibits the peripheral re-uptake of catecholamines like dopamine or noradrenalin resulting in central sympathetic stimulation, such as increased heart rate, blood pressure and bronchodilatation. This effect predestines ketamine in the anaesthesia of TBI, because of the injury-induced rise of intracerebral pressure (ICP). An increase of the ICP following a TBI is caused by reflective brain swelling, intracerebral haemorrhage or oedema. To avoid hypoperfusion of the brain during that phase, the increase of blood pressure caused by the ketamine has a neuroprotective effect.

A solution with 880 µl Ketasol and 620 µl Rompun was prepared, resulting in an injection solution containing 12.4 mg xylazine and 88 mg ketamine as hydrochloride per ml (18). A dosage of 1ml/kg bodyweight was used, leading to a 30-45 µl intraperitoneal injection of the prepared solution for each mouse with a bodyweight between 20-30 g. That resulted in an actual dose of 0.372 -0.558 mg xylazine and 2.64-3.96 mg ketamine hydrochloride per animal, depending on bodyweight.

To reduce the stress for the animals and to avoid abdominal injuries during the intraperitoneal (ip) injections, the mice were temporarily anaesthetized for 1~2 minutes with isoflurane with a flow of 1.8 l/min applied to a small box (~20cm x 30cm x cm15) (*Figure 6*).

The unconscious animals were placed on their back, with the right hind limb pulled slightly upwards to reach the intraperitoneal cavity with the needle, without having any abdominal organs at the injection site. All injections were made on the right half of the intraperitoneal space to avoid accidental injection into the big arteries located mainly in the left torso. (Aorta descendens, Arteria iliaca communis)

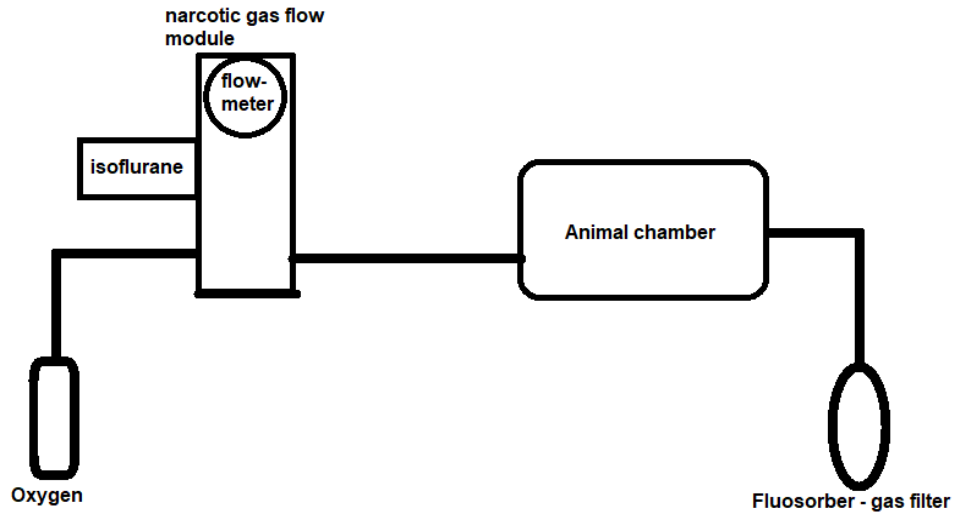

Figure 6: Schematic view of apparatus used for isoflurane anaesthesia

To avoid complications and reduce stress for the animal during intraperitoneal injections of BrdU, Ketamine-Xylazine solution (for i.p. anaesthesia) or Phenobarbital (for the sacrifice), animals were sedated with isoflurane gas.
The narcotic gas flow module equates a vaporizer and was filled with fluid isoflurane (Isofluran-Piramal). The proportioning of isoflurane conducted to the animal chamber via plastic tubes was controlled by a flow meter regulating the oxygen flow through the narcotic gas module (All components of the volatile anaesthesia equipment were from Rothacher, Switzerland). In order to avoid overdosing the animals the average oxygen flow was set to 1.8 l/min, leading to unconsciousness of the animals in ~ 1 minute.
From the animal chamber, the narcotic gas was channelled through plastic tubes into a Fluosorber (Veterinary Fluosorber, The Harvard Apparatus, United Kingdom), where the anaesthetics vapour was adsorbed.

After the injections, the animals were kept in their housing cages under an infrared lamp, until they were unconscious approximately 10 minutes later. When the corneal reflex and pain signs were not observed any more the mice were placed and fixed on the stereotactic frame for either a sham surgery or a trauma surgery and a modCCI.
17 out of 38 animals developed a reversible cataract within the first 30 minutes after the intraperitoneal injection of xylazine/ketamine. These cataracts were evaluated as a side effect of the xylazine (61) and were entirely reversible without further medical interventions within ~2 hours. To reduce the risk of irreversible

opacities, which would be a possible bias for the behavioural testing in the IntelliCage, eye management during surgery came into focus. The trans-corneal water loss combined with an altered aqueous humour composition due to corneal exposure was mentioned as a possible cause for the occurrence of the reversible cataracts (61).
Therefore Aquatears were applied to the eyes of the animals to prevent them from drying out and their eyes were covered with a foil to keep them in the darkness to avoid retinal damage during the time of surgery under surgical lamp. After recovery from anaesthesia, no signs of reduced eyesight were observed in any of the animals.
The dose of xylazine/ketamine seemed sufficient as no further incidents occurred during surgery (no raise of heart frequency or respiratory rate). After interventions (sham and trauma) animals were on a heating pad for 1-2 hours until fully recovered from anaesthesia to prevent hypothermia.

2.3.2 Surgery

For the surgery, animals were anaesthetized as described above (2.3.1). After getting unconscious and unresponsive to corneal and pain stimulus, the region needed for the incision was shaved (from in between the ears to the beginning of the nose bone) and the animals were fixed in the stereotactic frame with a metal spike from each side through the auditory canal into the os temporale and the maxilla was based on a metal bite plate. The fixation of the head must be stable and with the skull surface horizontal to drill the craniotomy. The eyes were kept wet with Aquatears and covered under foil before the shaved area was cleaned with 70% ethanol and beta-dine.
After disinfection, a 2 cm long longitudinal skin incision was performed right above the sagittal suture of the skull, from the posterior edge of the skull till an imaginary line between the eyes of the animal. The skin was held sideward with bulldog clamps to have the skull exposed. The periosteum in the opened area was removed with a periosteal elevator and occurring bleeding from the muscles or the skin was stopped by compression with 0.3% H_2O_2 -soaked cotton sticks.

2.3.3 Controlled cortical impact injury

After the periost removal, the coordinates of the planned craniectomy hole were marked. Therefore, the cranial sutures and the veins visible under the thin bone

(approximately 0.7-1 mm thick) were used as additional landmarks. The lesion site should be above the right hippocampus, resulting in a craniectomy site in the parietal bone approximately 1 mm lateral of the sagittal sinus in the posterior half of the distance between lambda and bregma (62). To avoid fatal injuries of the big blood vessels (sagittal sinus, right inferior vertebral vein or the transversal sinus) in this area, the craniotomy was not placed directly above the big blood vessels, visible through the cranium.

Before and during the drilling, the identified spot for the craniectomy was kept wet with sterile physiological saline (0.9% NaCl, Fresenius-Kabi, Austria) to ease the drilling by washing bone dust out of the craniotomy site as well as to avoid heat-induced damage. For the craniectomy, an electric drill was used with a hollow drill bit (4mm diameter). The drilling was stopped, when the hollow drill bit went almost through the bone, leaving just the lamina interna of the parietal bone intact. The remaining bone segment was flapped up with forceps and taken out to expose the dura mater. The craniectomy site was washed with sterile physiological saline to remove all of the bone dust before setting up the impact system, consisting of controller, the actual cortical impact device mounted to a stereotactic arm and the impact tip.

Therefore, a 3 mm diameter impact tip was screwed into the CCI arm which was fixed to the stereotactic frame. To generate a consistent trauma, the CCI-arm was brought with the impact tip right above the craniotomy hole. The surface of the brain was parallel to the surface of the impact tip. The parameters for the moderate trauma were as follows: 3 m/s velocity, 200 ms dwell time and 1 mm impact depth (18). The velocity and the dwell time were programmed at the controller module, while the depth had to be adapted by lowering the CCI arm that has been attached to the stereotaxic frame. For this purpose, the impact tip was brought into the extended position, and a negative electrode was attached to the animal’s neck. The impact tip was slowly moved towards the brain surface until contact was indicated by an alarm. The impact tip was pulled back into the retracted position and then the CCI arm was moved 1 mm downwards to have the 1 mm impact depth upon firing.

After impact, 2 out of 18 animals had a breathing arrest and were excluded. The impact site was not washed out after trauma, only the skin incision was closed with

single knot stitches carefully to protect the opened brain from mechanical or infectious posttraumatic damage.
Animals were kept on a heated blanket to prevent them from hypothermia for the first hours after trauma.
Sham animals have undergone through the same surgical procedure except craniectomy and controlled cortical impact.

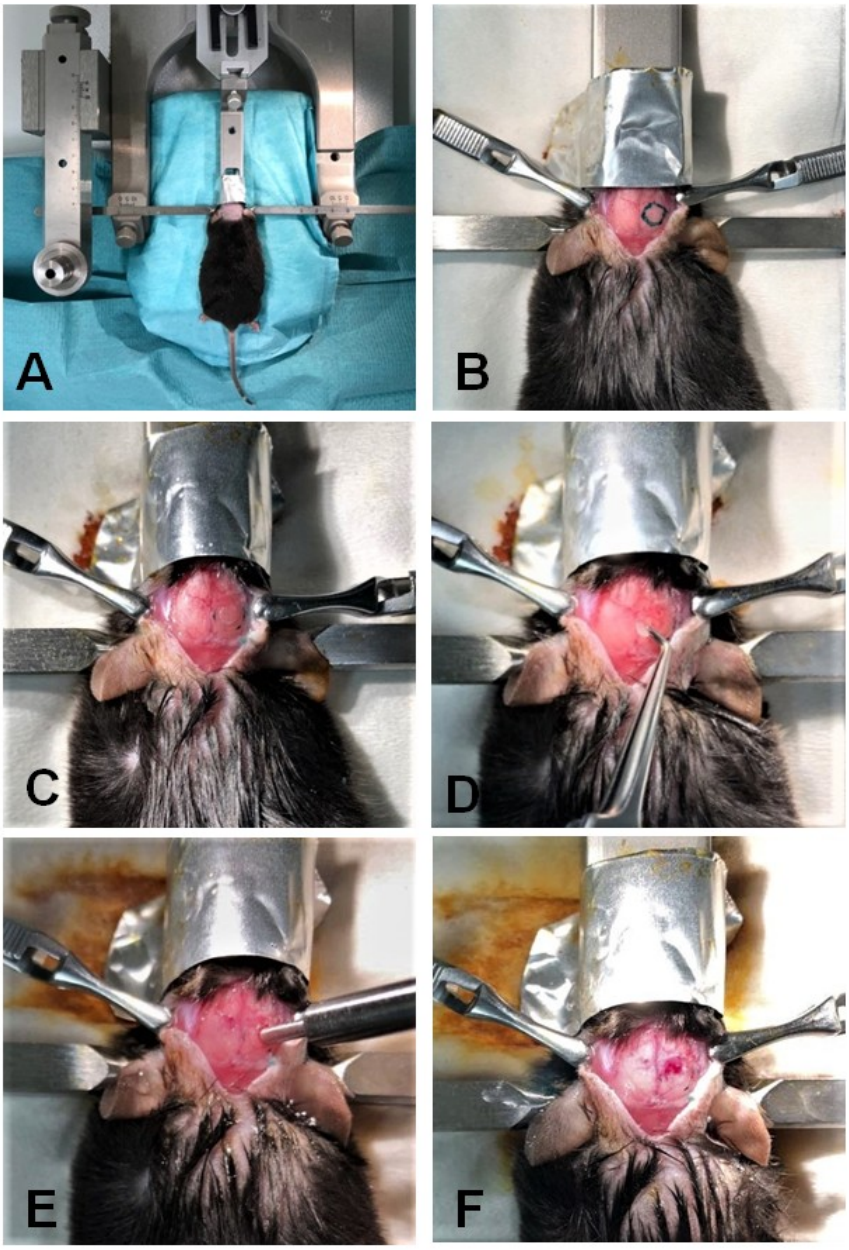

Figure 7: Surgery and CCI

*The skull of the anesthetised and shaved animal was fixed in a stereotactic frame (**A**), and after disinfection with alcohol pads and beta-dine a 2 cm long skin incision was made and the periosteum was removed. The marked site for the craniectomy (**B**) was around 1 mm lateral from the sagittal suture to the right parietal bone. The drill was stopped, before it made its way through the entire bone (**C**). With a thin forceps, the remaining skull piece at the craniectomy site was gently lifted and flapped away (**D**). The piston tip was installed in a 90 degree angle above the exposed surface of the brain (**E**) to have a consistent trauma. After the trauma (**F**) no additional interventions were made, and the skin was closed with single knot sutures.*

2.3.4 Post-surgical treatment

Post-surgical treatment focused on antibacterial prophylaxis and pain reduction. Therefore, the animals received Carprofene for pain management and Enrofloxacin as antibiotic prophylaxis (*Figure 8*).

Carprofene is a non-steroidal anti-inflammatory drug (NSAID) which was subcutaneously injected right after the surgery while the animals were still under anaesthesia and on day 1 and 2 for post-surgical pain relief. At each injection, a dosage of 20 mg/kg bodyweight was administered (63). To get this low dose of ~50 µg/animal (20-30 g bodyweight), 50 µl Carprofen (50mg/ml; Rimadyl, Pfizer Corporation Austria GmbH, Austria) Rimadyl was diluted in 10 ml 0.9% NaCl. Every animal got 200 µl of the prepared Rimadyl/NaCl dilution subcutaneously injected at the neck.

Enrofloxacin is a fluoroquinolone antibiotic and widely used in antibacterial treatment in rodents. A dose of 5 mg/kg bodyweight was injected subcutaneously right after the surgery and on day 1. To inject a dose of 5mg/kg bodyweight 50µl enrofloxacin solution (25mg/ml, Baytril, Bayer Vital GmbH, Germany) was diluted in 2 ml 0.9% NaCl, and 200 µl of the dilution was injected subcutaneously in the neck.

Animals were closely observed the first days after the surgery or the trauma and the suture was controlled and if necessary cleaned with beta-dine from day 1 until day 7 after surgery. All occurring health issues in the animals were reported to the veterinarian and if necessary, the animals were treated or excluded.

2.3.5 BrdU Injection

For the labelling of the post-traumatic produced neurons, 1 mg of Bromodeoxyuridine (BrdU) was administered intraperitoneally. BrdU is an analogue of the nucleoside thymidine widely used in the labelling of proliferative cells. BrdU can later be detected by anti-BrdU specific antibodies during immunohistochemistry (64).

For the *in vivo* labelling in the mice, a 10 mg/ml solution of BrdU in sterile DPBS was used. (BD Pharmingen™ Bromodeoxyuridine Cat: 550891, BD Biosciences). For the injection, the mice were sedated with isoflurane gas in a small chamber (see anaesthesia). When sedated an injection with 100 µl of BrdU solution (10 mg/ml of BrdU in 1X DPBS) was intraperitoneally administered for 7 days, equivalent to a daily dose of 1 mg BrdU from day 2 until day 8 after trauma.

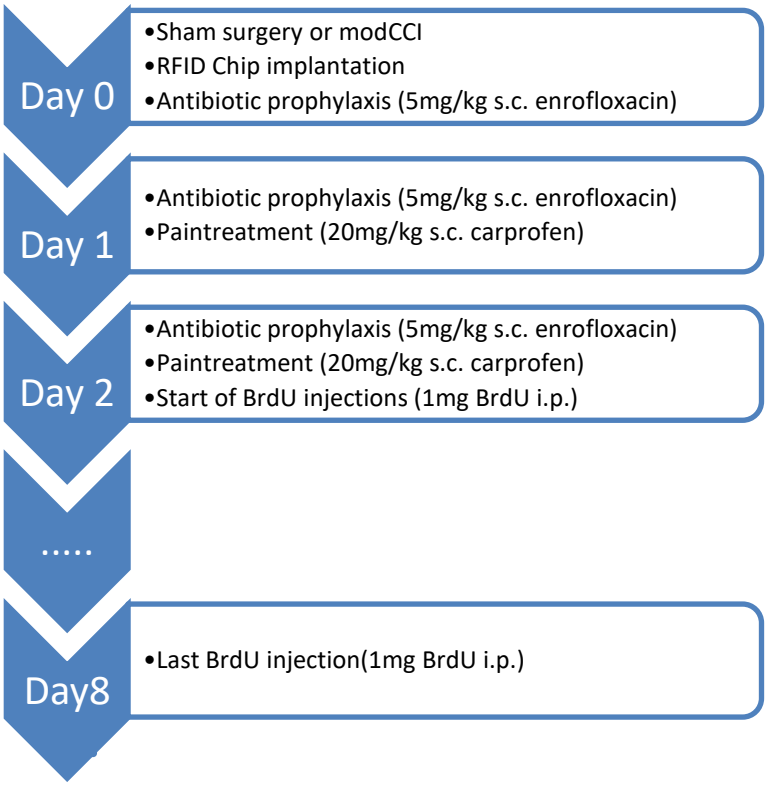

Figure 8: Overview of post-surgical treatment

2.4 Assessment of learning and memory in the automated home cage environment

For this purpose, the IntelliCage system of "NewBehaviour AG, Zürich" was used. This IntelliCage module consists of a 20 cm high laboratory rodent cage with a 62x44 cm top surface containing a metal food grid and a 55x38.5 cm ground surface. The ground surface is covered with litter and a housing shelter is placed inside to convey a home-cage environment during the tests (65,66).

For testing the spatial memory, it was crucial, that the cage was not moved throughout the experiment, with two significant objects visible from the inside on two sides of the cage for better orientation. A 12hours /12hours dark/light circle was used for each group with light from 06.00 to 18.00 and the temperature in the cage during the experimental phases was between 21.5 and 23.5°C.

Each edge of the rectangular-shaped cage contains a ***sensor apparatus*** made up of two entrance holes with 3 cm diameter each, an RFID antenna for animal identification, a temperature sensor, which recognizes animal's presence, a door system with integrated infrared light beams, which can register nosepokes and two 250 ml drinking bottles as well as lick sensors surrounding the drinking nipples.

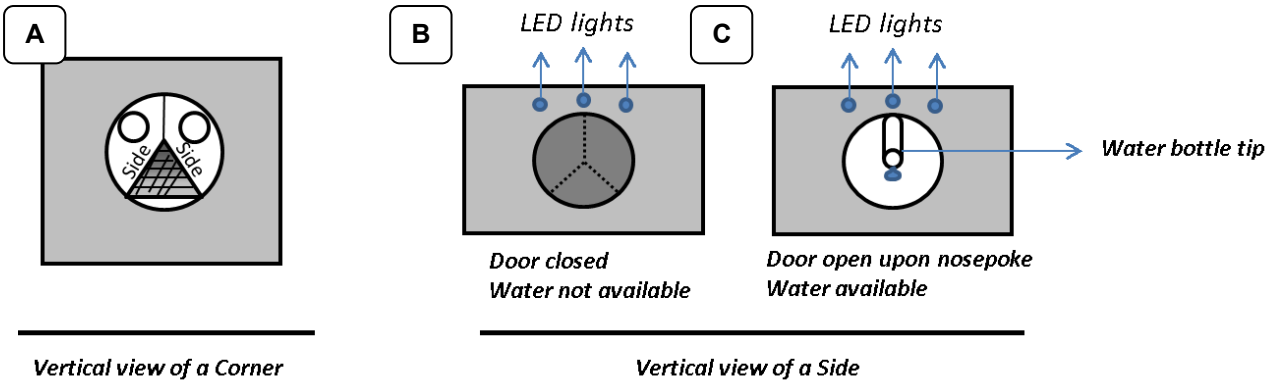

Figure 9: Schematic view of the corners with the sensor and actor set up.
*To identify the visiting animals, an RFID sensor is mounted to the entrance hole. Each entrance-hole leads to two sides (**A**) of the corner which are separately closable by a motorized door (**B**). The doors can be opened by a nosepoke, registered by a temperature sensor and an infrared light beam. Three LED lights above the doors can give the animal a visual feedback for either a right or wrong visit (red or green light signal) (**B, C**). Each side (2 per corner) leads to two water bottle nipples, with lickometers counting the licks of the drinking animal (**C**). An air-puff valve is also integrated into the corners.*

Besides the sensor set up, an ***actor set up*** is also integrated into the IntelliCage, consisting of three different LEDs per side, an air-puff valve (max. 3.5 bars) and a motorized door system for each of the two sides per corner (*Figure 9)*.
When an animal entered its correct corner, a green LED lit, while entering a wrong corner resulted in a red LED shining. The moment the RFID antenna and the temperature sensor registers the presence of an animal, a countdown of 300 seconds starts, which would lead to an air-puff to prevent the animals from sleeping or spending a lot of time inside a favourite corner, which would make it unavailable for others and would lead to bias.
These components not only allow a great variety of different test setups to monitor different aspects of behaviour but also to train and observe spatial and behavioural learning.

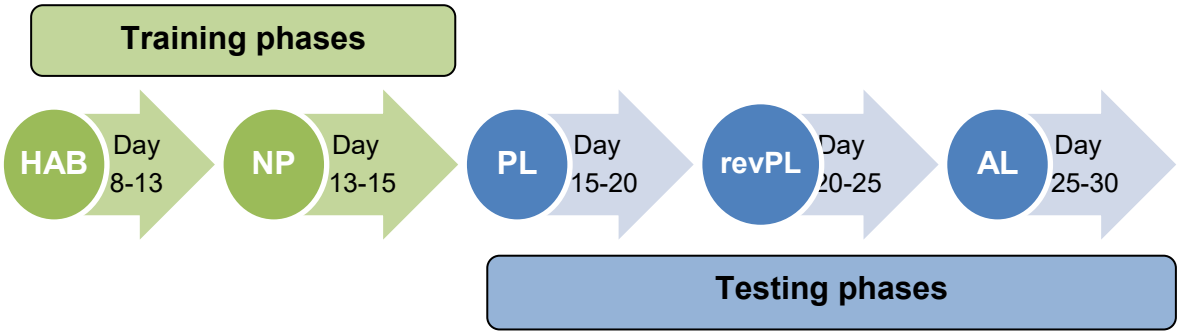

Figure 10: Timeline of the phases in IntelliCage set-up

*Habituation (**HAB**) and nosepoke (**NP**) phases were established to habituate the animals to the new environment and they had to learn that water-bottle tips are only accessible by nose-poking the doors.Place learning (**PL**), reversed place learning (**revPL**) and avoidance learning (**AL**) were the actual testing phases, where visits, nosepokes and licks were recorded for statistical analyses.*

The IntelliCage phase for the animals lasts from day 8 until day 30 after trauma, consisting of 5 different phases (*Figure 10*). The first phase was a habituation (HAB) phase, to accustom the mice to the new environment, without any regulations, food and water provided *ad libitum*. The second phase was the nosepoke (NP) phase, where animals had to learn how to trigger the mechanism to open the doors, blocking the way to the drinking bottles. In these two phases the corners were all neutral and drinking was allowed all the time, so that each animal was free to visit and drink at any corner at any time of the day *ad libitum.*
In the following phases, access to the water bottles was restricted to two different time slots during the dark phase; from 00.00 until 01.00 and from 05.00 until 06.00, to have a stronger exogenous motivator to achieve learning performance.
The third phase was the place learning (PL) phase, where every mouse got access to the water bottles in only 1 out of the 4 corners and drinking was allowed only during testing phases (*Figure 11*). The fourth phase was the reversed place learning (revPL) phase, similar to the place learning phase, but the “correct” corner, where they were allowed to drink, changed diagonally. The last testing phase was the avoidance learning (AL) phase, where incorrect visits during the allowed drinking period was penalised by a 1 bar air-puff.
The first two phases (HAB, NP) were designed to train the animals to the needed tasks they would have to fulfil in order to access the water bottles in the actual testing phases (PL, revPL, AL). With this test setup, an insight on various aspects

of learning performance, including spatial, operant and aversive learning was expected.

The activity of the animals was recorded from the HAB phase on, consisting of three events:

1. Visits → counted by the RFID antenna at the entrance to each corner and a positive presence signal through the temperature sensor
2. Nosepokes → registered by an infrared light beam in front of the closed doors, upon the touching of the mouse to the door with his nose.
3. Licks → counted by a lickometer, triggered by the animals licking attempts at the bottle tip

The visit and nosepoke baseline from the HAB (visit only) and the nosepoke phase were used to assign each mouse to a corner for the PL phase, which was selected as the least preferred corner. When too many animals have the same least visited corner, then corners with the least preferred nosepoke was chosen. This was made to avoid assigning them to corners they might have voluntarily preferred during the HAB or NP phase.

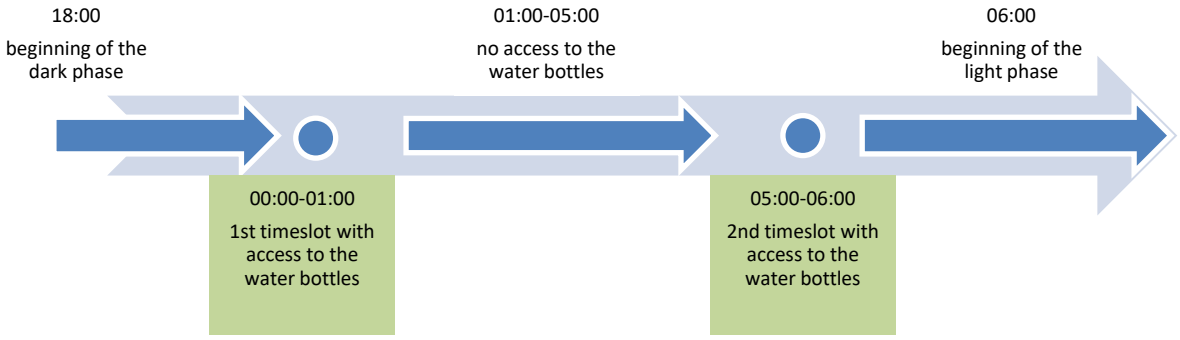

Figure 11: Drinking slots during testing phases

Time slots during the testing phases independent of "correct" or "incorrect" drinking attempts.

Exclusion criteria in the IntelliCage were as follows: 1) Lack of a visit in the first 24 hours. 2) In case of at least one corner visit, lack of drinking in a period of 48 hours.

After surgery, the animals were kept in the same groups and cages like before, to avoid postsurgical stress induced by a new environment. Furthermore, the BrdU ip injections were planned to take place before the transfer to the IntelliCage.

On day 30 after surgery or trauma, animals were taken out of the IntelliCage and housed again in conventional cages, until the sacrifice on day 45 after trauma.

2.4.1 RFID Chips

For assigning the actions recorded by the various sensors in the IntelliCage radiofrequency identification (RFID) transponder was implanted subcutaneously at the neck of each mouse on the day of the surgery, while the animals were still under anaesthesia, to reduce additive stress and risk caused by additional sedation for chip implantation.

Therefore, the chip-containing needle was inserted in a skin fold of the neck, at least 1cm away from the craniectomy hole to avoid the accidental dislocation to the exposed surface of the brain. After implanting the RFID chip, the injection canal was closed with a single knot suture, to prevent the animal from losing the chip while scratching or cleaning their head and neck. Nevertheless, 2 of 38 implanted chips had to be re-implanted, before the behavioural testing started.

With these RFID chips, each mouse got a personalized identification number, so the performance of the animals was individually recorded during the whole experiment.

The RFID transponders were explanted when the animals were sacrificed.

2.5 Phases in the IntelliCage

2.5.1 Habituation phase

On day 8, shortly before the start of the dark/night phase, the animals were moved to the IntelliCage. The HAB phase lasts for 5 days, until day 13, to habituate the animals to their new environment.

The doors of the corners were all open continuously, so the animals had free access to water in every corner to get used to the cage (Figure 12). In this phase, no additional restrictive rules were set up.

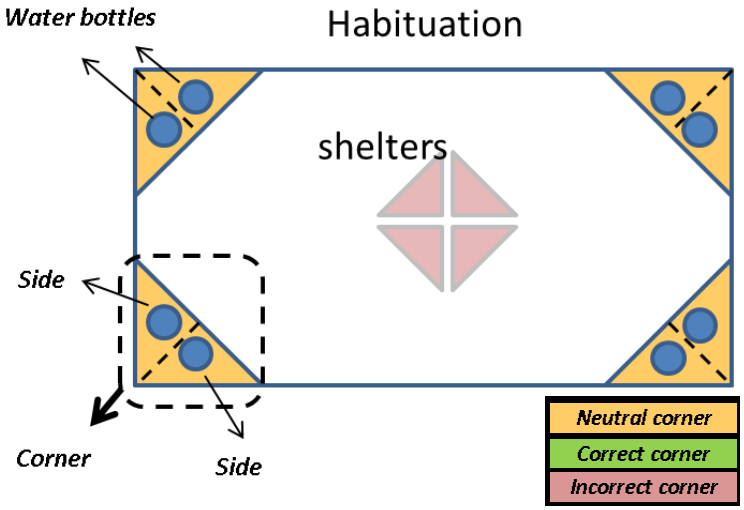

Figure 12: Habituation phase

Schematic view of the habituation phase, with all corners assigned as "neutral" (free access to the water bottles placed at two sides of each corner)

2.5.2 Nosepoke phase

For further testing, it was crucial, that the animals learn how to open the doors, which block the way to get access to the water bottles. During the nose poke phase, instead of free access, a door blocks the holes which lead to the bottles. The doors opened in response to a nosepoke and were closed again after 10 seconds. To trigger the nosepoke sensor, animals had to push their nose against the door blocking their way to the bottles, in order to open the doors. In this phase, no restrictions on the location of the corners were made, meaning each mouse was allowed to drink from every corner if the nose poke was sufficient. This phase was from Day 13-15 after trauma.

2.5.3 Place learning

The PL phase was designed to test the spatial memory of the animals, knowing its dependence on hippocampal activity and functionality (67,68).

This first testing phase, where the animals were forced to learn, starts on day 15 after surgery or trauma and lasts for 5 days until day 20 after trauma. In this phase, the animals had to learn and remember that there is only one out of the four corners, where they could open the door and access the water by nose poking (*Figure 13*).

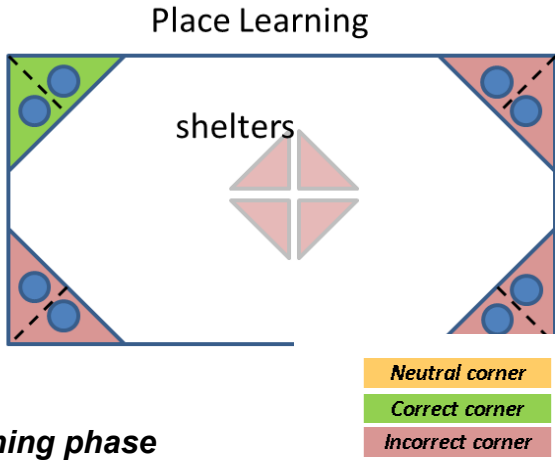

Figure 13: Place learning phase

Schematic view of the place learning phase; one correct corner (green) and three incorrect corners (red) for each animal.

The mice were grouped into four groups, with one corner defined as the “correct” and the three remaining corners defined as “incorrect”.
During the drinking slots, animals entering the correct corner could open the door by nose-poking and gain access to the water, while in the “incorrect” corners they would not be able to open the door.

2.5.4 Reversal Place Learning

After the PL phase, the revPL began, which lasts from day 20 until day 25, to examine the capability of the animals to form new spatial memory. The definition of correct and incorrect corners was changed to the diagonal opposite, compared to the PL phase (*Figure 14*).

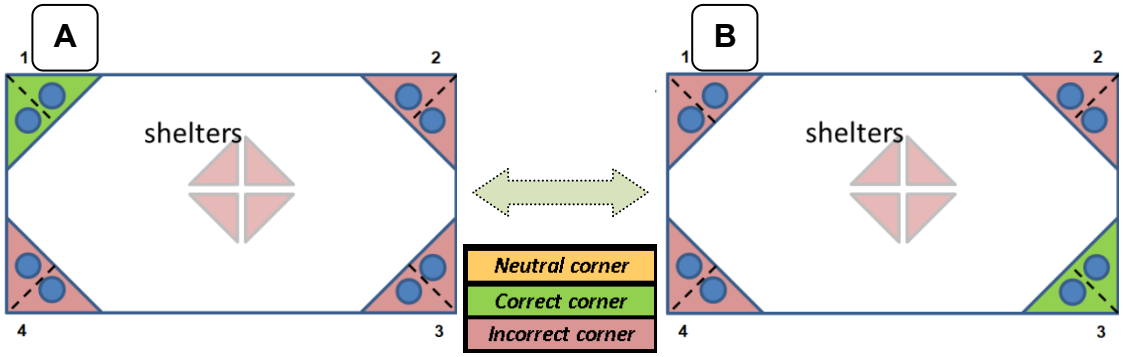

Figure 14: Assigning to corners

*Between the testing phases, the corners were changed diagonally at the beginning of each phase (revPL and AL). In **A** the correct corner (green) was **1**, in **B** (symbolising the following testing phase) the correct corner was **3**. Same procedure was used for corners **2** and **4**.*

2.5.5 Avoidance learning

The Avoidance Learning phase starts on day 25 and lasts until day 30, meaning animals have been in the IntelliCage for 17 days.

This phase was designed to test a combination of spatial, operant and aversive learning at once. Animals were allowed to visit all corners freely, but during drinking slots, a 1 bar air-puff would be triggered upon visiting an “incorrect” corner (*Figure 15*). Nose-poking the “correct” corner would again give them access to the drinking nipples of the water-bottles(69).

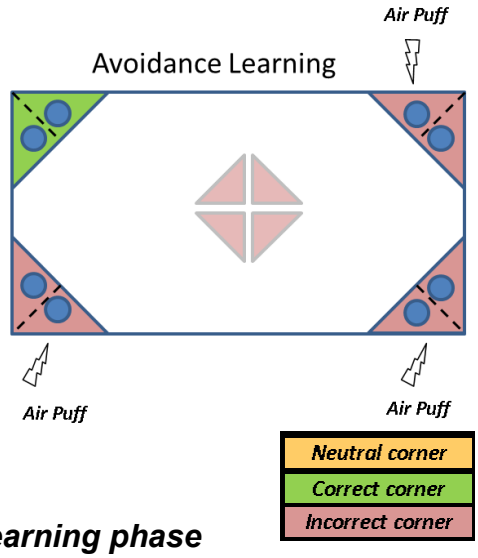

Figure 15: Avoidance learning phase

Schematic view of the cage setup at avoidance learning phase. Visits of corners defined as “incorrect” (red) triggers an air puff at the entrance hole.

2.5.6 Learning performance and spatial memory

In order to find functional differences among the experimental groups the percentages of incorrect visits and nosepokes of each animal were calculated. A place error was defined as the registration of the animal's presence at an incorrect corner and a nosepoke error was defined as the presence signal and the activation of the nosepoke sensor at an "incorrect corner".

The data from the IntelliCage was exported as tab-delimited text files. In order to calculate percentage of incorrect visits, percentage of incorrect nosepokes and the drinking performance of the animals, the number of total and incorrect visits and nosepokes, and as well the number of licks during drinking phases were extracted from the recorded data using a Python script that was developed with the great help of Nikolaus Kopp, BSc. of the University of Technology Graz. Then the data was tabularized using Microsoft Excel 2010 and prepared for further statistical analyses.

The four different time slots (described in method behavioural testing) were evaluated separately over 4 days; day-by-day (18:00-18:00), dark phase (18:00-06:00), night phase (00:00-06:00) and the actual testing phase (00:00-01:00 and 05:00-06:00).

Furthermore, the ratio of place or nosepoke *[errors at the interim phase (01:00-05:00) / errors at the drink phase (00:00-01:00 and 05:00-06:00)]* were compared among the groups to assess possible disturbances of short-term memory.

The revPL and the AL phase were not included into the statistical evaluation in consequence of an incident, which occurred during the revPL phase of the miR451$^{-/-}$ modCCI group, making further interpretation unreliable.

2.6 Euthanasia and Sample Collection

All animals were sacrificed on day 45 after the surgery or trauma with intraperitoneal injection of ~0.1 ml pentobarbital (400 mg/ml, Richter Pharma, Austria) following a temporary sedation with isoflurane.

Deep anaesthesia was confirmed with the absence of reflexes to the pain stimuli (paw pinch) before opening the thorax for the transcardial perfusation. Then the animal was fixed with needles to a styropor base, the front limbs spread apart. As a surgical approach for accessing the heart, the skin was carefully removed from the ventral thorax. A horizontal incision caudal of the xiphoid was made, followed by cutting through the ribs left and right parasternal (estimated 1 cm lateral of the

sternum on each side). The ventral thorax fragment was folded up and fixed with a clamp to have a sufficient view of the heart in the thoracic cavity (70).
While the heart was still beating, a ~2 mm cut was made to the dorsal part of the apex and the perfusion-catheter was introduced into the left ventricle and carefully pushed up till the tip of the catheter was visible in the aortic arch.
The visible tip of the infusion-catheter was manually fixed with a forceps and the formalin (3.7% formaldehyde in sterile PBS) infusion was started with a speed of 1 drop (equals ~ 0.06 ml) per second. Then the right atrium was opened by an incision to allow optimal perfusion.
Through the fixed catheter the 3.7% FA in PBS solution was slowly infused to the animal for 2~4 min, depending on the various signs of adequate FA perfusion of the animal, like the colour of the liver, muscle contractions, and stiffness as the reaction to arriving FA. Mainly, the change of colour in the liver served as an indicator for successful transcardial FA perfusion.

2.7 Preparations for histological analysis

After the transcardial perfusion, the animals were decapitated at the atlanto-occipital joint. The skin, muscles and other remaining tissue was removed to have a sufficient view of the skull and the brain visible underneath. A 1mm sagittal cut to the centre of the occipital-bone was made at the imaginary extended sagittal suture. The tips of the scissors were pushed gently in between the two nasal bones. By rotating the scissors 90 degrees and opening them, the skull breaks at the sagittal suture and the brain was exposed. Then, the brain was gently detached from the skull base by dissecting the *chiasma opticum* and any brain nerves visible and the brain was taken out and put into a 10 ml Falcon tube, filled with 3.7% FA in PBS. The samples stayed 24 hours at +4°C in the 3.7% FA, then the solution was changed to PBS following wash with PBS (twice), and stored in 1X PBS at +4°C until the histological preparations (71).
For the cryo-sectioning of the samples, the 1X PBS solutions was removed and the brains were soaked in 15% sucrose for 24 hours. Then the brains were snap-frozen using a cryospray containing pressurized propane and butane (Medite Medizintechnik, Germany). The frozen brains were fixed on the sample holder using an embedding medium for frozen tissue specimens that contain water soluble glycols and resins (Tissue-Tek, Sakura, Japan). Tissue slices were prepared as frozen coronal sections in 20 µm thickness using Microm HM 560 M

(Microm GmbH, Walldorf, Germany). To have frozen sections of a bigger area of interest on each of the slides, the sections were collected alternating with 5 different object slides resulting in 4 sections of the brain on each slide with 100 µm in between representing a 300 µm thick segment of the mouse brain.
Cryo-cut sections were left to air dry at room temperature overnight and then the slides were stored at -20°C until further analysis.

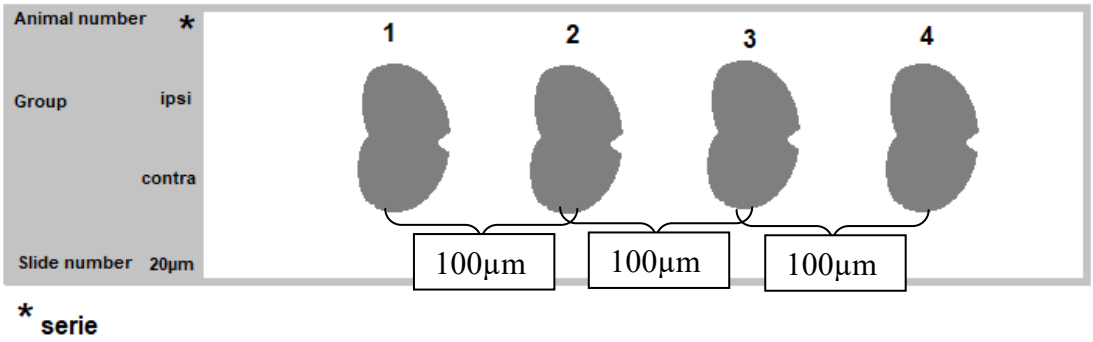

Figure 16: Labelling of slides

The labelling of slides included animal number, the series number (*), the group (e.g. wt-sham), the slide number within the series. The thickness (20µm) and the sides (ipsi- and contralateral) were also noted on the object slide.
*4 consecutive sections of the brain (**1-4**) were fixed on each slide, with 100µm sagittal gap between the sections.*

2.8 Immunostaining

For histological analysis, the staining of the incorporated BrdU, which was administered intraperitoneally from day 2 until day 8 after trauma, was used to detect newly proliferated cells.
Thymidine analogues like Bromodeoxyuridine are commonly used for immunohistochemical visualization of newly proliferated cells (72–74). The *in vivo* BrdU labelling of cells complies with the principle of integration of the BrdU during DNA synthesis, where BrdU is incorporated instead of the nucleoside Desoxythymidine triphosphate. Various experiments using BrdU labelling of newly proliferated cells following trauma have shown the promotive impact of TBI on cell proliferation in the dentate gyrus (10). As BrdU is an unspecific marker for cell proliferation, not discriminating between different cell types and classes, a second, specific marker was needed to selectively detect neuronal cells.

In this study, NeuN (neuronal nuclei protein) was used, to label the mature neurons. NeuN is a neuron-specific protein expressed for the most part in the cell nuclei and partly at the perinuclear cytoplasm, as it is part of the nuclear matrix of most mature neuronal cells in mammals (75,76).
First described in 1992 by Mullen et al. (75) NeuN has been broadly used to mark functional/mature neurons in various studies (17,22,74,76,77). The selectivity of NeuN for nervous tissue is appreciably higher as other neuronal differentiation markers, as it is restricted to neurons, while neuron-specific enolase or synaptophysin are not only expressed by neurons, but also by neuroendocrine cells (78). An additional benefit of NeuN as a marker is its selectivity for maturated neurons as it is absent in immature neural progenitor cells while they are still in the cell cycle (78,79).

2.8.1 Co-immunostaining of BrdU and NeuN positive cells

For the co-immunostaining of the BrdU and NeuN, the slides with the 20 µm thick coronary slices of the hippocampus were taken out of the -20°C storage and kept in their storage boxes for 30 minutes at room temperature. To guarantee the comparability of the analyzed brain sections, slides from the ventral, medial and dorsal part of the hippocampus were used.
For post-fixation, slides were put into 3.7% FA (formaldehyde) in PBS (phosphate-buffered saline) for 10 minutes. Then, the slides were washed in a shaker 3 times for 5 minutes in PBS. 10 mM sodium citrate buffer (pH 6.0) was used for antigen retrieval, as FA-induced protein cross-linking causes most of the epitopes unavailable. Therefore the samples were soaked in the heated 10 mM sodium citrate buffer for 3 minutes, followed by 3 times of 5 minutes washing in PBS in a shaker. Since BrdU is located in the nuclei, 30 min incubation in 2N HCl was utilized to permeate the nuclear membrane. To rebalance the pH after HCl treatment, the slides were soaked/drenched in 0.05 M Borat buffer for 6 minutes followed by 3 times 2 minutes PBS wash at a shaking platform.
Then the block solution (5% horse serum in 0.3% Triton X-100 in PBS) was applied for 1 hour in a humidified chamber to reduce non-specific antibody binding. As primary antibody for the BrdU, a 1 to 1000 dilution of sheep anti-BrdU (abcam ab1893-1.3mg/ml) in block and for the NeuN, a 1:1000 rabbit anti-NeuN (abcam ab104225) in block were applied onto the samples overnight at +4°C.

Before the application of the secondary antibody, samples were washed 3 times for 5 minutes in 0.3% Triton X-100 in PBS in a shaker. During the following steps exposure to the light was avoided to protect fluorophores that are conjugated to the secondary antibodies from bleaching. Donkey anti-sheep IgG Alexa 647 (abcam ab150179, 1:500 in block) and a donkey anti-rabbit IgG Alexa 488 (abcam ab150061, 1:1000 in block) were applied for 1 hour at room temperature.
Before final processing, the samples were washed again in 0.3% Triton X-100 in PBS. Then a 4′,6-Diamidin-2-phenylindol (DAPI) containing aqueous mounting media (Fluoroshield™with DAPI, Sigma-Aldrich, Germany) was applied on the samples and the slides were covered with the coverslips and sealed with a nail polisher to protect samples from drying.

2.8.2 Microscopy

Microscopy was performed using Axio Imager 2.1 (Carl Zeiss AG, Oberkochen, Germany) installed with TissueFaxs Cell Analysis System (TissueGnostics GmbH, Vienna, Austria). All pictures were taken with a 20x magnification lens and 3 different light channels for separate wavelengths according to the different emission of the fluorophores conjugated to the secondary antibodies as well as for DAPI. Therefore, a far-red channel was used to detect the Alexa 647 (BrdU), a green channel was used to detect IgG Alexa 488 (NeuN) and a blue channel was used for visualizing DAPI staining.

2.8.3 Image Analysis

In order to count the newly proliferated cells, which were stained with BrdU and to count the BrdU and NeuN positive cells as newly proliferated neurons, the pictures were merged with the open source software ImageJ 1.46r (Schneider et al 2012). The three different pictures of one hippocampal region were merged into one picture with different colour channels. The resulting picture coloured the BrdU positive cells red, the DAPI positive cells blue and the NeuN positive cells green.

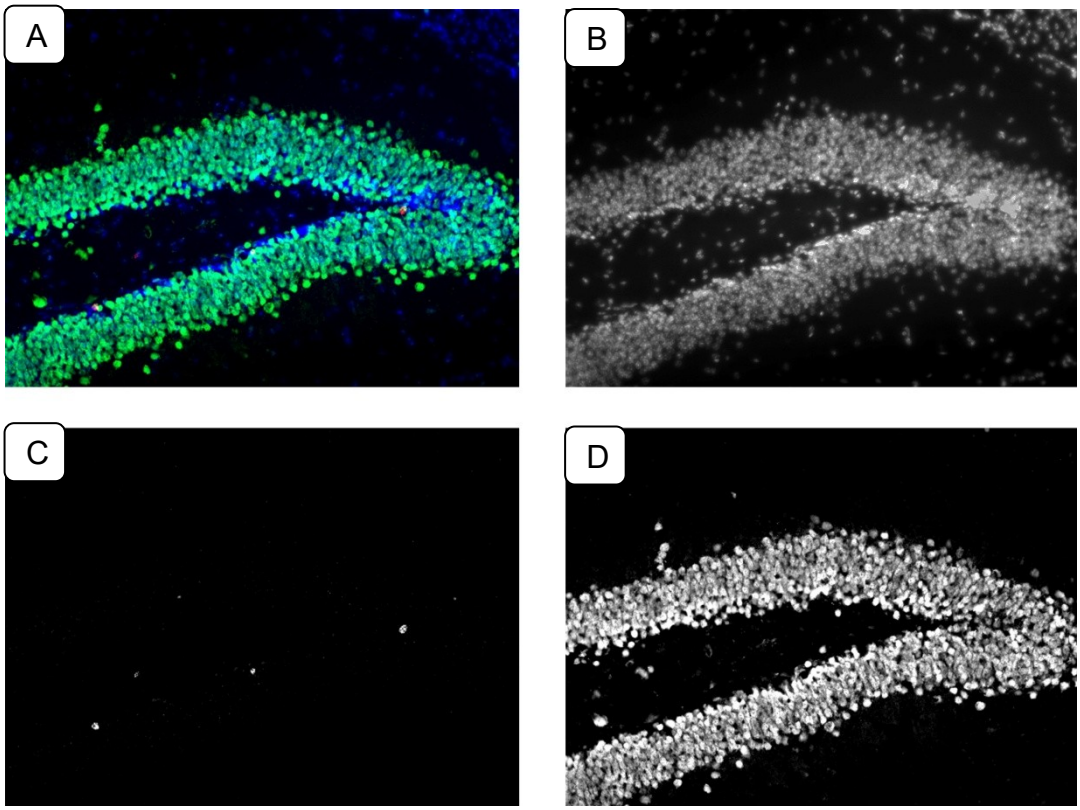

Figure 17: Overview of pictures used for discriminating BrdU positive cells from BrdU and NeuN positive cells.

The merged picture (A) was made by combining the three pictures from the DAPI channel (B) in blue, the BrdU channel (C) in red and the NeuN channel (D) in green.

The decision, whether a cell is BrdU+ or double positive, was based on the inspection of each single channel picture and the appearance of the target cell in the multichannel picture.

The BrdU and the double positive cells were counted in the whole pictured areal of the dentate gyrus and the surrounding hippocampal tissue of both sides (ipsilateral and contralateral). Therefore positive cells were counted by localisation; the hilus or dentate gyrus (*Figure 18*).

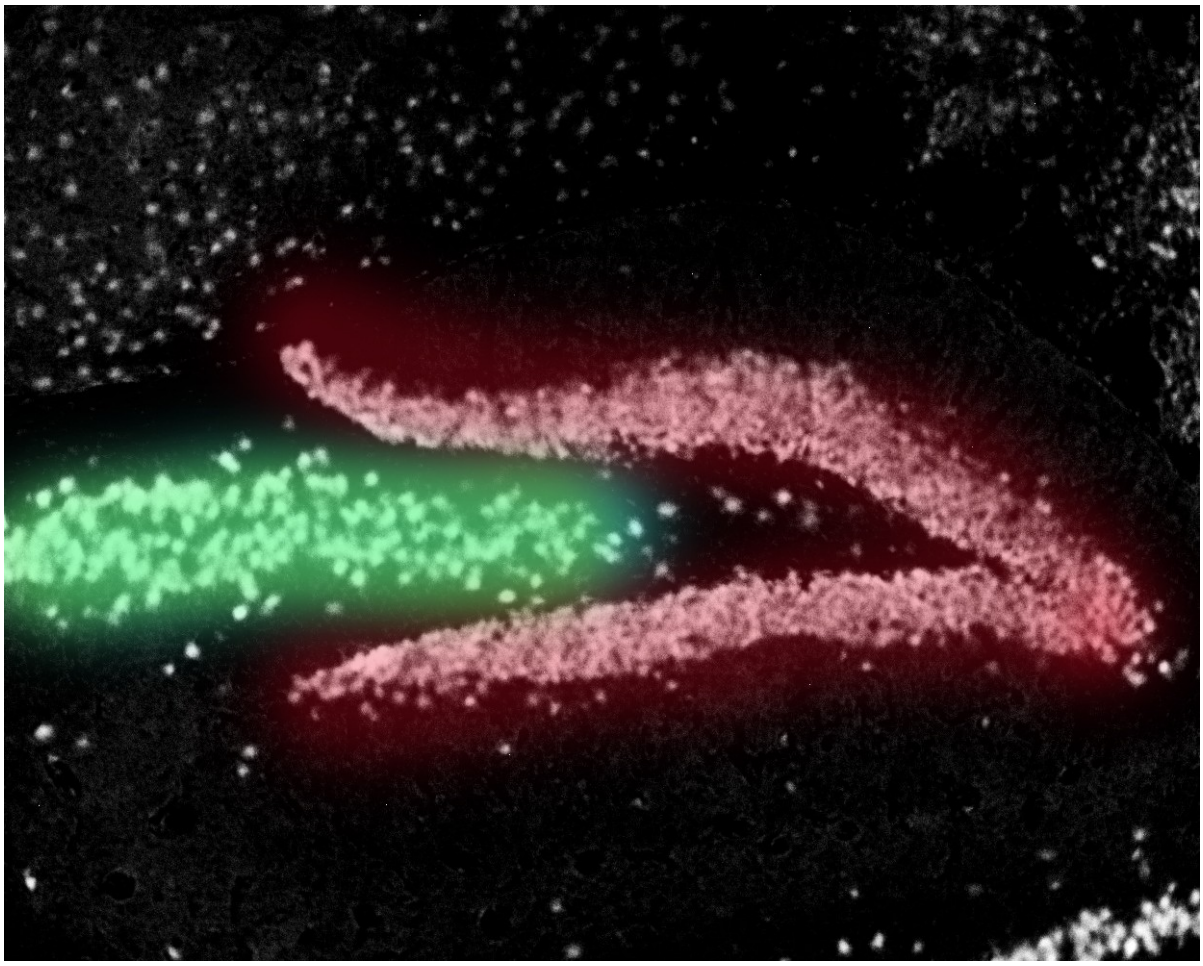

Figure 18: Overview of dentate gyrus and hilus

Schematic view of the separation into dentate gyrus (red) and hilus (green) region used in the counting of BrdU and BrdU/NeuN positive cells.

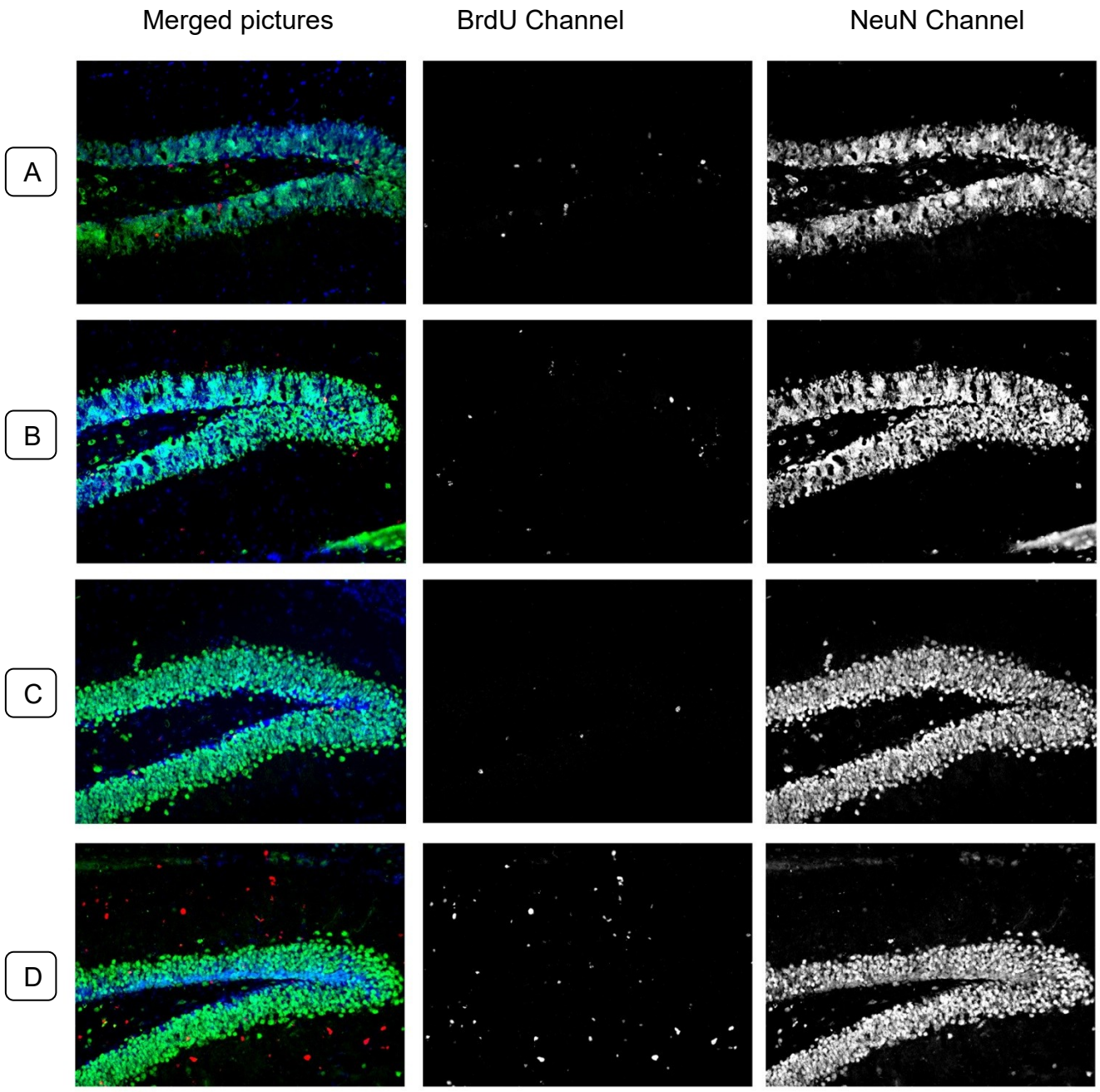

Figure 19: Representative overview of ipsilateral dentate gyrus

*Wild-type sham (**A**), wild-type modCCI (**B**), miR451$^{-/-}$ sham(**C**) and miR451$^{-/-}$ modCCI (**D**)*

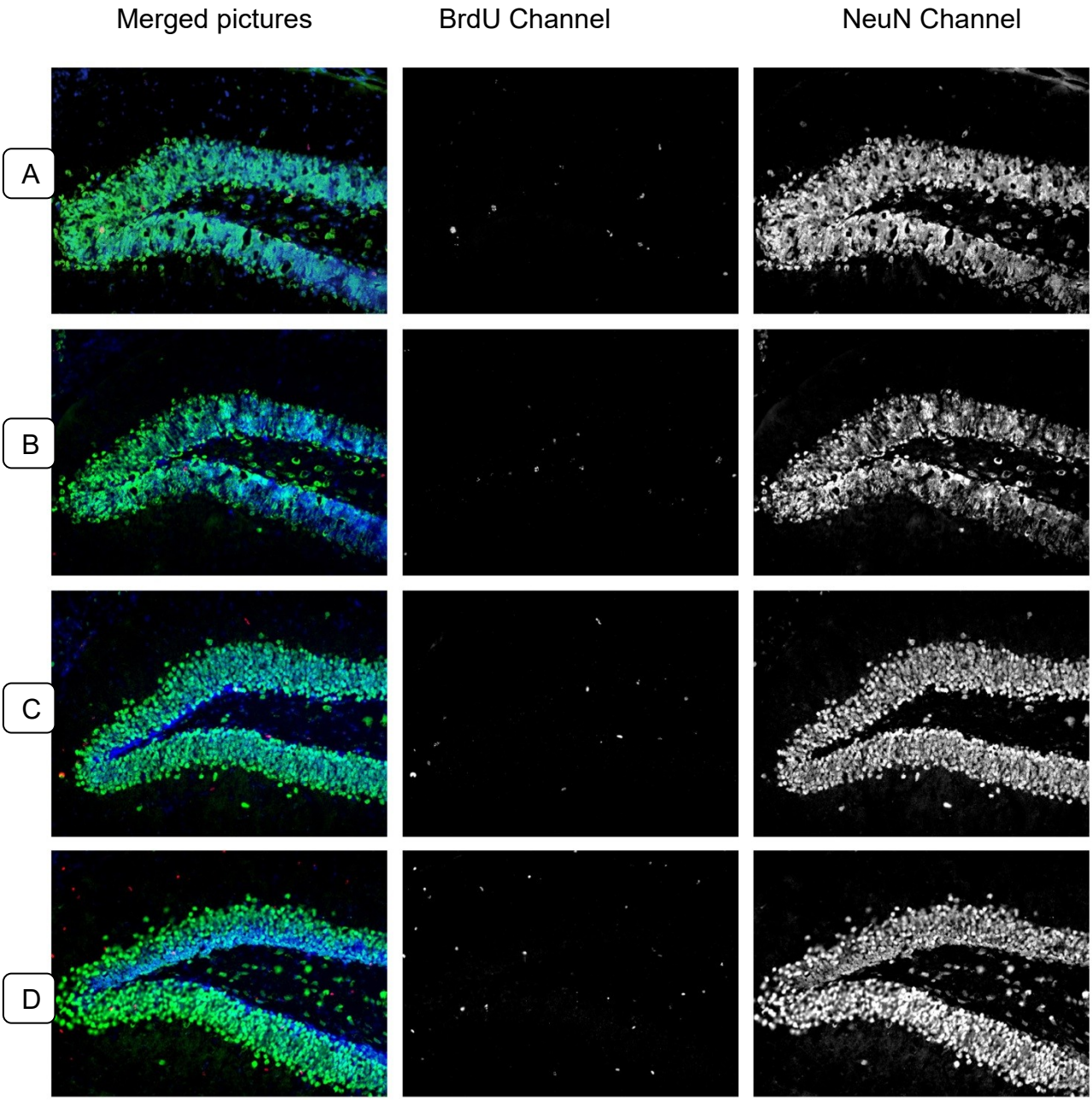

Figure 20: Representative overview of contralateral dentate gyrus

*Wild-type sham (**A**), wild-type modCCI (**B**), miR451$^{-/-}$ sham(**C**) and miR451$^{-/-}$ modCCI (**D**)*

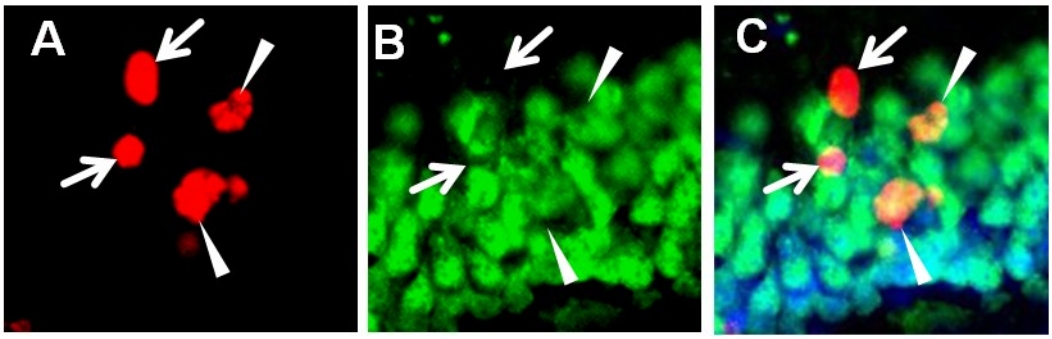

Figure 21: Representative example for discrimination of positivity

*The decision whether a BrdU positive cell (red) was also NeuN positive (green)double positive was based on the appearance of the cell in BrdU (**A**) and NeuN (**B**)channel. Also the overall appearance in a merged picture with DAPI (blue) (**C**) was taken into account. The arrows show examples of only BrdU positive cells, the arrowheads show examples of double positive signals.*

2.9 Data analysis

2.9.1 Cell proliferation and differentiation

Proliferation of cells after the trauma was verified by counting of BrdU positive cells in the dentate gyrus. Successful differentiation into mature and functional integrated neurons was examined by counting of BrdU and NeuN positive cells. The morphological and immunofluorescent appearance of each positive cell was evaluated individually. For the evaluation of differences in the proliferation and differentiation of cells in the dentate gyrus, BrdU and BrdU/NeuN positive cells were counted in 4 different individuals of the 4 experimental groups; wild-type sham, wild-type modCCI, miR451$^{-/-}$ sham and miR451$^{-/-}$ modCCI, in at least 4 consecutive coronal sections of the hippocampal area. Cell counts were tabularized in Microsoft Excel 2010 (Microsoft Corporation, Redmont, Washington, USA) and prepared for further statistical analyses.

Data is presented as box-whisker plots, the interquartile range was represented as the box, the median value was represented by a bar in the box; whiskers represent minima and maxima.

2.10 Statistical analyses

Statistical significance of the differences observed in BrdU+/NeuN+ cells was assessed using non-parametric tests. Numbers of double positive cells were

compared between sham and modCCI groups separately for each genotype using Mann-Whitney U Test.

The percentages of incorrect visits or nosepokes were compared either between the treatment groups separately for each genotype (wt: sham vs modCCI; miR451$^{-/-}$: sham vs modCCI) or between the genotype groups separately for each treatment (sham: wt vs miR451$^{-/-}$; modCCI: wt vs miR451$^{-/-}$).

Statistical significance of the differences observed in place errors and nosepoke errors were tested with mixed-model repeated measures ANOVA. Main effects were set as “Time” and “Treatment/Genotype”. In the absence of a Time X Treatment or Time X Genotype interaction, interpretation of the main effects was performed according to the results of the statistical output. In case of a significant interaction, main effects were evaluated separately using repeated measures ANOVA followed by pairwise comparison of incorrect visits/nosepokes for learning over time, and one-way ANOVA for comparison of different treatments or genotypes. In case of multiple comparisons, p-values were adjusted using Bonferroni correction.

Variance homogeneity across different groups was tested with Levene’s Test. Sphericity was assessed using Mauchly’s Test. In case of a violation of sphericity assumption, Greenhouse-Geisser correction was used.

All statistical analyses were performed by Muammer Üçal, PhD from the Research Unit of Experimental Neurotraumatology at the Medical University of Graz using SPSS Statistics Software Package (v.25, IBM, USA). In all comparisons, a p-value ≤0.05 was deemed statistically significant.

3 RESULTS

3.1 Post-TBI neurogenesis was more pronounced in miR451$^{-/-}$ mice

3.1.1 Dentate Gyrus

Post-TBI cell proliferation and neurogenesis in the dentate gyrus of hippocampus was evaluated with BrdU labelling of newly produced cells and co-immunostaining of BrdU and NeuN in the ipsilateral (*Figure 22*) and contralateral regions (*Figure 23*) at 45 days after sham surgery or moderate CCI in wild-type and miR451$^{-/-}$ mice. Then the number of BrdU+ cells (*Figure 24*) and double positive (BrdU+/NeuN+) cells (*Figure 25*) were quantified in both regions.

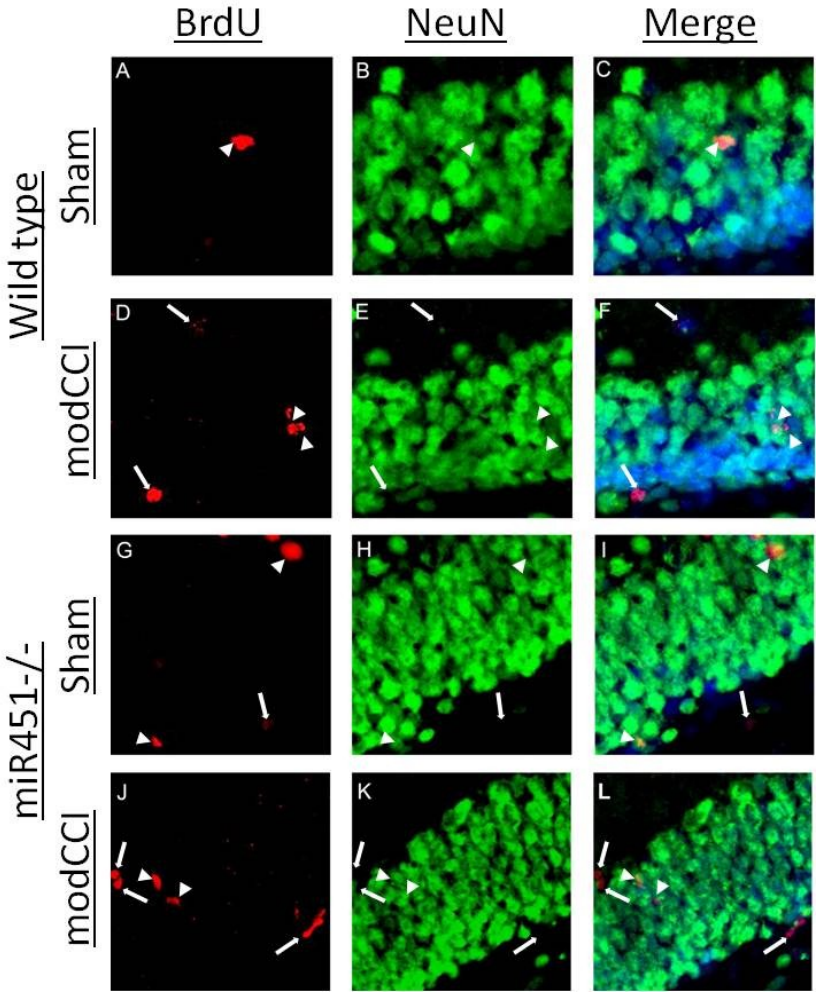

Figure 22: BrdU+/NeuN+ positive cells shown in ipsilateral dentate gyri

*Representative pictures showing BrdU+ and NeuN+ cells in ipsilateral dentate gyri of wild-type (wt) sham (**A-C**), wt modCCI (**D-F**), miR451$^{-/-}$ sham (**G-I**) and miR451$^{-/-}$ modCCI (**J-L**) animals. Arrows indicate BrdU+ cells (red), arrowheads indicate double positive cells. Cell nuclei were stained with DAPI for counterstaining.*

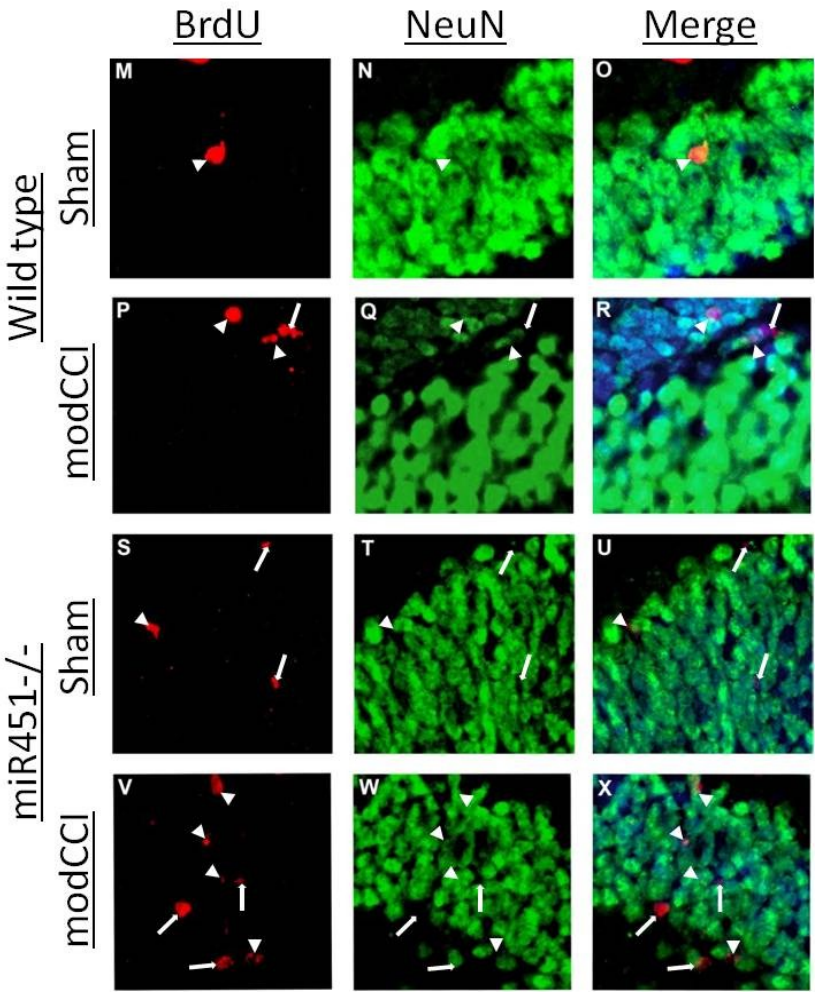

Figure 23: BrdU+/NeuN+ positive cells shown in contralateral dentate gyri

*Representative pictures showing BrdU+ and NeuN+ cells in ipsilateral dentate gyri of wild-type (wt) sham (**M-O**), wt modCCI (**P-R**), miR451$^{-/-}$ sham (**S-U**) and miR451$^{-/-}$ modCCI (**V-X**) animals. Arrows indicate BrdU+ cells (red), arrowheads indicate double positive cells. Cell nuclei were stained with DAPI for counterstaining.*

The total number of BrdU+ cells in the ipsilateral dentate gyri of wild-type animals was statistically not different after a moderate CCI (19.06±10.56) than those of respective sham controls (11.08±2.90, *p=0.556*). However, the number of BrdU+ cells was significantly higher in the ipsilateral dentate gyri of miR451$^{-/-}$ animals after a moderate CCI (25.23±10.02) as compared to the respective sham controls (7.63±1.76, *p=0.016*) (*Figure 24* A).

In the contralateral dentate gyri, significant increases in the number of BrdU+ cells were observed after moderate CCI both in the wild-type (13.19±4.81, *p=0.032*) and miR451$^{-/-}$ animals (18.52±6.35, *p=0.016*) as compared to the sham controls (**wt:** 8.57±2.21; **miR451$^{-/-}$**: 8.60±3.12) (*Figure 24* B).

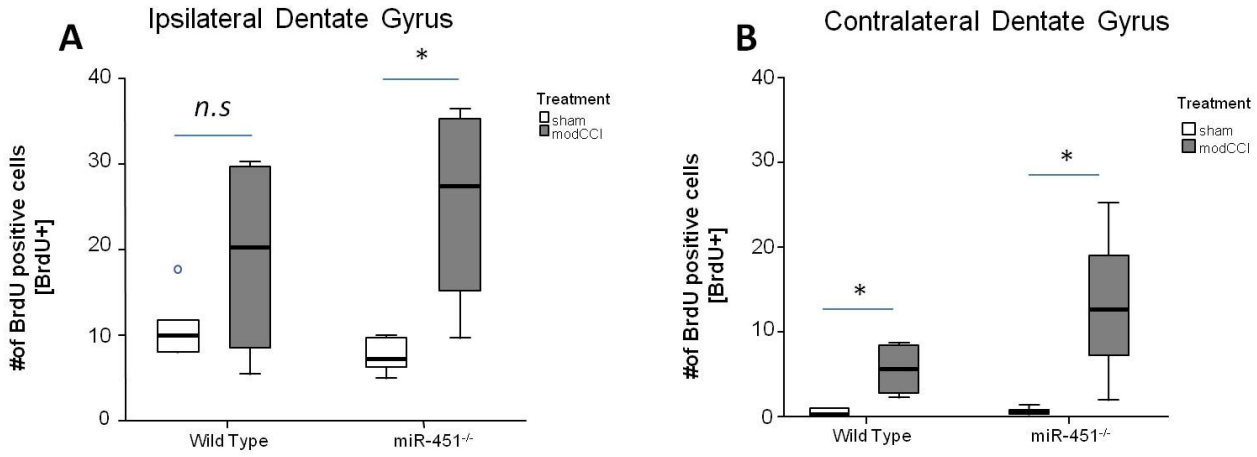

Figure 24: Quantification of BrdU+ cells in the Dentate Gyrus of hippocampus of wild-type and miR451$^{-/-}$ mice.

*Numbers of BrdU+ cells are shown in dentate gyri of **A**) ipsilateral and **B**) contralateral hippocampi. In wild-type group, the number of BrdU+ cells was significantly increased only contralateral to the injury, while miR451$^{-/-}$ animals showed increased number of BrdU+ cells in both sides after a moderate CCI. Statistical significance of the observed differences (Sham vs modCCI for each genotype) was tested with Mann-Whitney U Test. *p<0.05, n.s.: not significant.*

Next, the numbers of double positive cells (BrdU+/NeuN+) were compared among different groups in order to have a better understanding of the post-traumatic neurogenesis in wild-type and miR451$^{-/-}$ brains (*Figure 26*).

The numbers of BrdU+/NeuN+ positive cells in the ipsilateral dentate gyri of modCCI groups were not significantly different than those of respective sham controls either in the wild-type (**sham**: 3.47±1.89, **modCCI**: 5.94±3.53, *p=0.556*) or in the miR451$^{-/-}$ animals (**sham**: 4.15±1.12, **modCCI**: 9.04±4.08, *p=0.730*) (*Figure 28Figure 25* A).

In the contralateral dentate gyri a statistically significant difference in the number of double positive cells was not observed in wild-type modCCI animals (4.44±2.31) compared to the sham controls (3.27±1.25, *p=0.111*). However, in the miR451$^{-/-}$ animals, there was significantly higher number of double positive cells in the contralateral dentate gyri of modCCI animals (6.77±3.60) compared to the respective sham group (4.77±0.82, *p=0.016*) (*Figure 25* B).

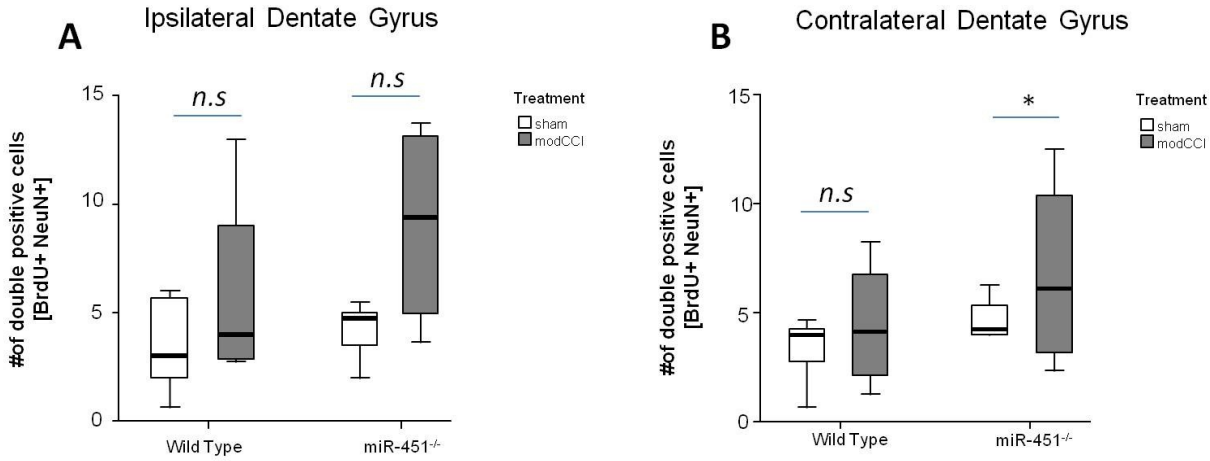

Figure 25: Quantification of BrdU+/NeuN+ cells in the Dentate Gyrus of hippocampus of wild-type and miR451$^{-/-}$ mice

*Post-TBI neurogenesis was assessed with BrdU and NeuN co-immunostaining in dentate gyri of **A**) ipsilateral and **B**) contralateral hippocampi. More BrdU+/NeuN+ cells were observed in miR451$^{-/-}$ animals after CCI, although the sham groups of both genotypes showed comparable number of double positive cells. Statistical significance of the observed differences (Sham vs modCCI for each genotype) was tested with Mann-Whitney U Test.*p<0.05, n.s.: not significant.*

3.1.2 Hilus

Under physiological conditions newly born neurons in the SGZ migrate to the granular layer of dentate gyrus. Nevertheless, we observed newly born neurons in the hilus as well, particularly in the animals with brain injury, in both the ipsilateral (*Figure 26*) and the contralateral sides (*Figure 27*).

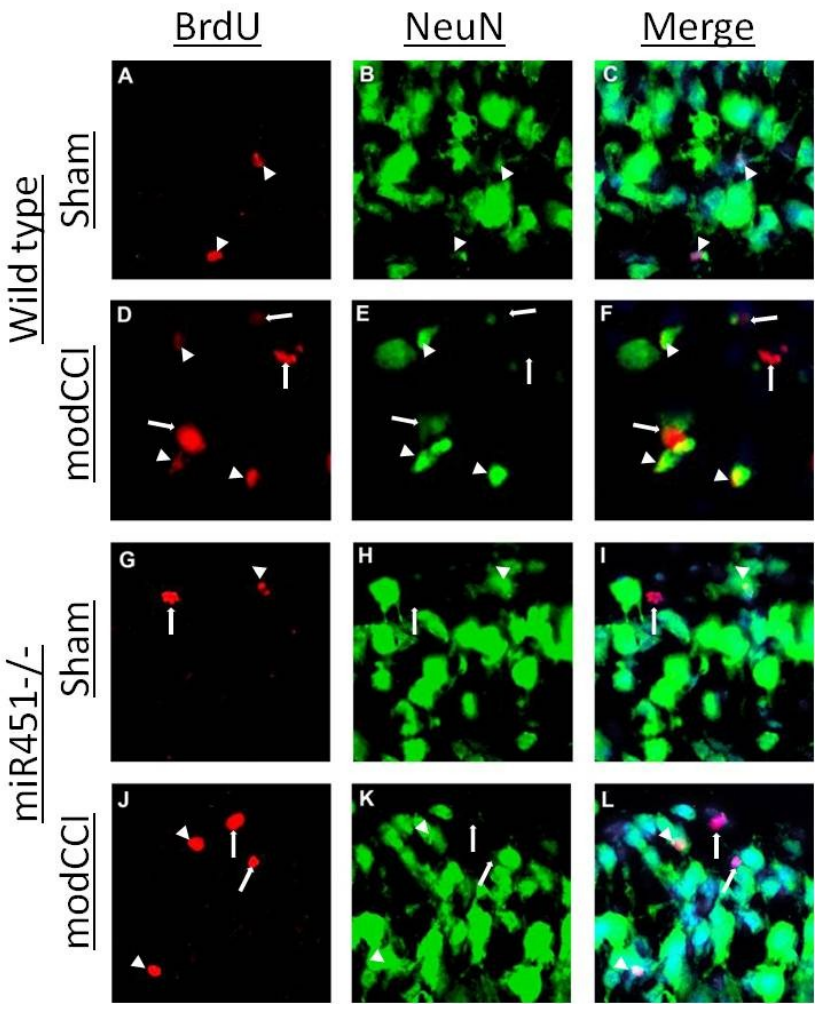

Figure 26: BrdU+/NeuN+ positive cells shown in ipsilateral hilus

*Representative pictures showing BrdU+ and NeuN+ cells in the ipsilateral hili of wild-type (wt) sham (**A-C**), wt modCCI (**D-F**), miR451$^{-/-}$ sham (**G-I**) and miR451$^{-/-}$ modCCI (**J-L**) animals. Arrows indicate BrdU+ cells (red), arrowheads indicate double positive cells. Cell nuclei were stained with DAPI for counterstaining.*

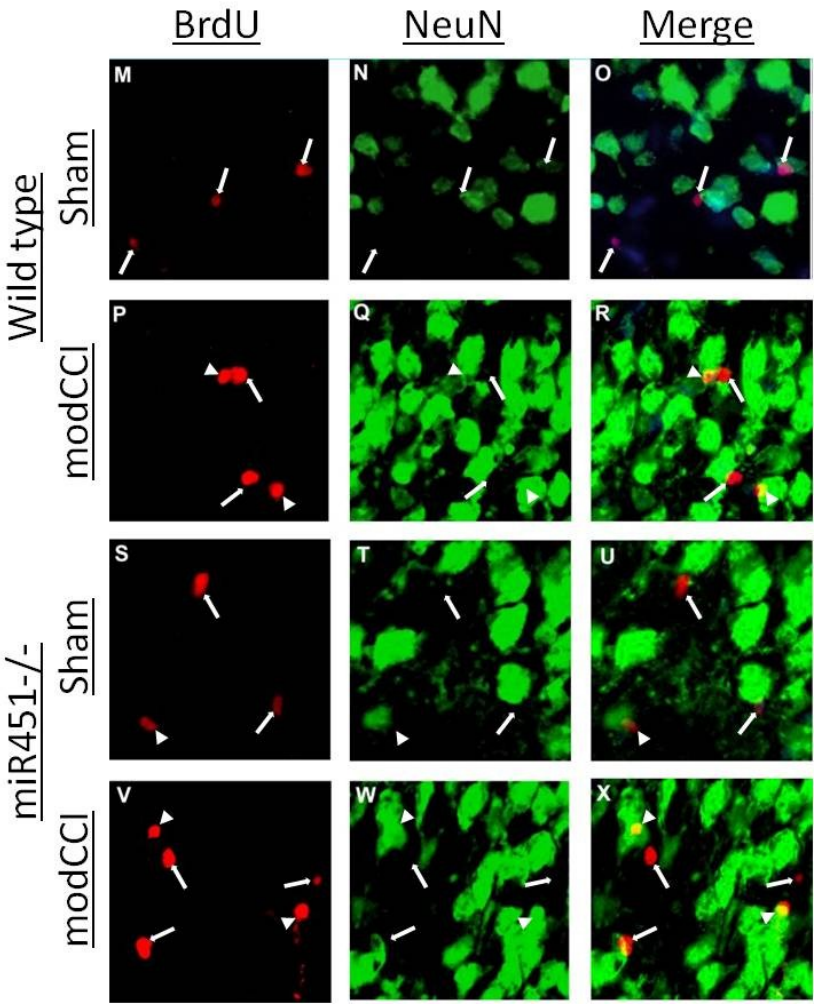

Figure 27: BrdU+/NeuN+ positive cells shown in contralateral hilus

*Representative pictures showing BrdU+ and NeuN+ cells in contralateral hili of wild-type (wt) sham (**M-O**), wt modCCI (**P-R**), miR451$^{-/-}$ sham (**S-U**) and miR451$^{-/-}$ modCCI (**V-X**). Arrows indicate BrdU+ cells (red), arrowheads indicate double positive cells. Cell nuclei were stained with DAPI for counterstaining.*

The total number of BrdU+ cells in the ipsilateral hilus of modCCI groups were not significantly different than those of respective sham controls either in the wild-type (**sham**: 0.25±0.30, **modCCI**: 0.50±0.50, p=*0.286*) or in miR451$^{-/-}$ animals (**sham**: 0.12±0.14, **modCCI**: 1.90±1.18, *p=0.190*) (*Figure 28* A).

In the contralateral hilus, the increases in the number of BrdU+ cells was not statistically significant in the wild-type animals with moderate CCI (0.13±0.13) compared to the respective sham controls (0.10±0.16, *p=0.063*). However, in the miR451$^{-/-}$ animals there was a significantly higher number of BrdU+ cells in the

contralateral hilus after modCCI (7.79±2.21) compared to the sham controls (0.47±0.43, *p=0.008*) (*Figure 28* B)

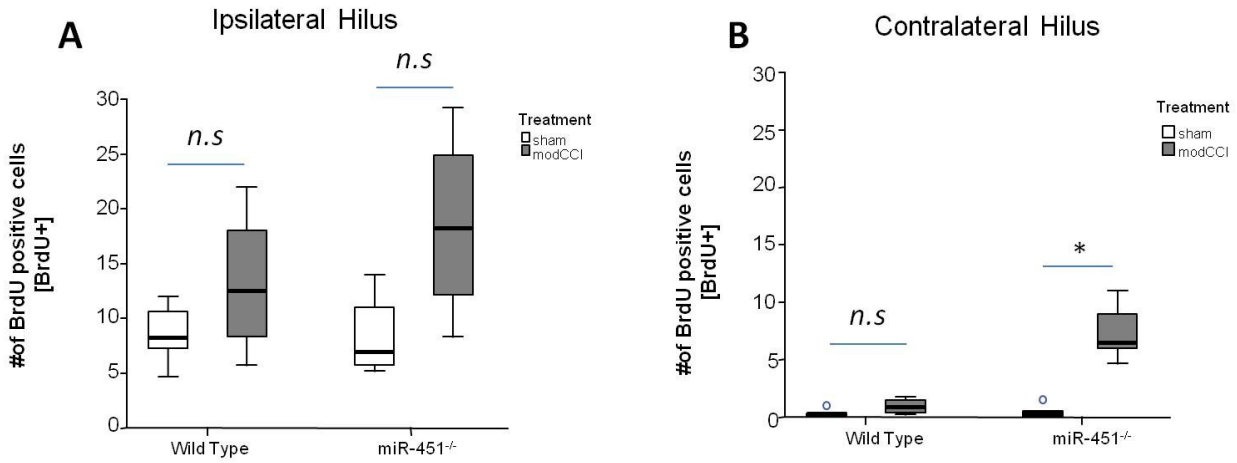

Figure 28: Quantification of BrdU+ cells in the hilus region of wild-type and miR451$^{-/-}$ mice.

*Numbers of BrdU+ cells are shown in the hilus of **A**) ipsilateral and **B**) contralateral hippocampi. TBI-induced increases observed in the miR451$^{-/-}$ animals were more pronounced in both ipsi- and contralateral regions, but statistically significant only at the contralateral side. Statistical significance of the observed differences (Sham vs modCCI for each genotype) was tested with Mann-Whitney U Test. *p<0.05, n.s.: not significant.*

To assess whether these newly proliferated cells detected in the hilar regions were differentiated into neuronal phenotype, the numbers of BrdU+/NeuN+ cells were compared among the different groups.

The numbers of double positive cells in the ipsilateral hilus of modCCI groups were not significantly different than those of respective sham controls either in the wild-type (**sham**: 0.25±0.30, **modCCI**: 0.50±0.50, *p=0.556*) or in miR451$^{-/-}$ animals (**sham**: 0.12±0.14, **modCCI**: 1.90±1.18, *p=0.730*) (*Figure 29* A).

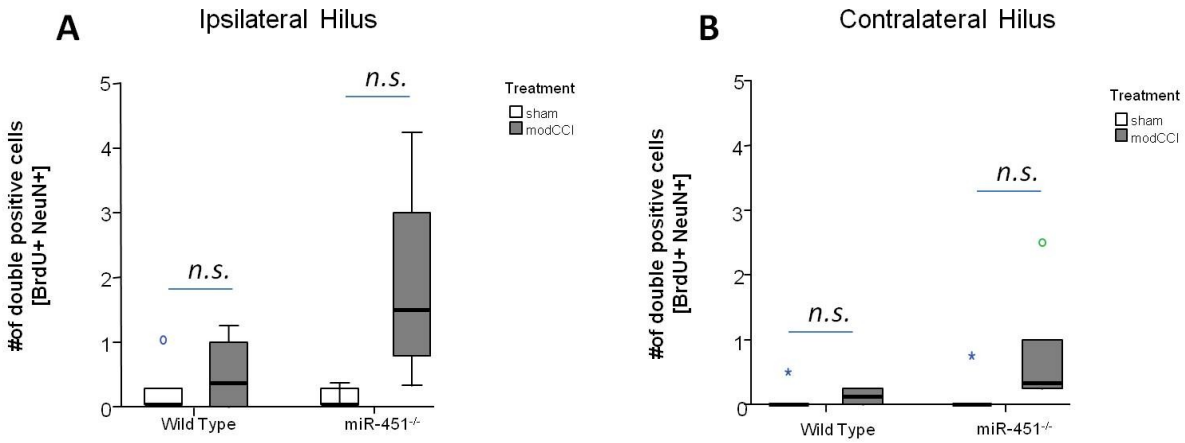

Figure 29: Quantification of BrdU+/NeuN+ cells in the hilus region of wild-type and miR451$^{-/-}$ mice.

*Numbers of double positive cells are shown in the hilus of **A**) ipsilateral and **B**) contralateral hippocampi. TBI-induced increases observed in the miR451$^{-/-}$ animals were more pronounced in both ipsi- and contralateral regions, but the differences did not reach to the statistical significance. Statistical significance of the observed differences (Sham vs modCCI for each genotype) was tested with Mann-Whitney U Test. n.s.: not significant.*

In the contralateral hilus a significant increase in the number of double positive cells was not observed in wild-type and miR451$^{-/-}$ modCCI groups (**wt**:0.13±0.13, **miR451$^{-/-}$**: 0.83±0.83) compared to the sham controls (**wt**:0.10±0.16, *p=1.00*, **miR451$^{-/-}$**:0.15±0.24 *p=0.056*). But notably the increases in the miR451$^{-/-}$ group was very close to the statistical significance level (*p=0.056*) (*Figure 29*B).

3.2 Changes in Learning and Memory Performance in IntelliCage After moderate Controlled Cortical Impact (CCI) Brain Injury

In order to evaluate the post-TBI changes in the learning performance and spatial memory in wild-type and miR451$^{-/-}$ animals, we analysed the place errors and nosepoke errors in the place learning phase of the IntelliCage.

3.2.1 Place Errors:

When their activity was analysed on a 24-hour basis, differences were observed between place learning performance of the wild-type and miR451$^{-/-}$ animals after moderate TBI (Figure 30)

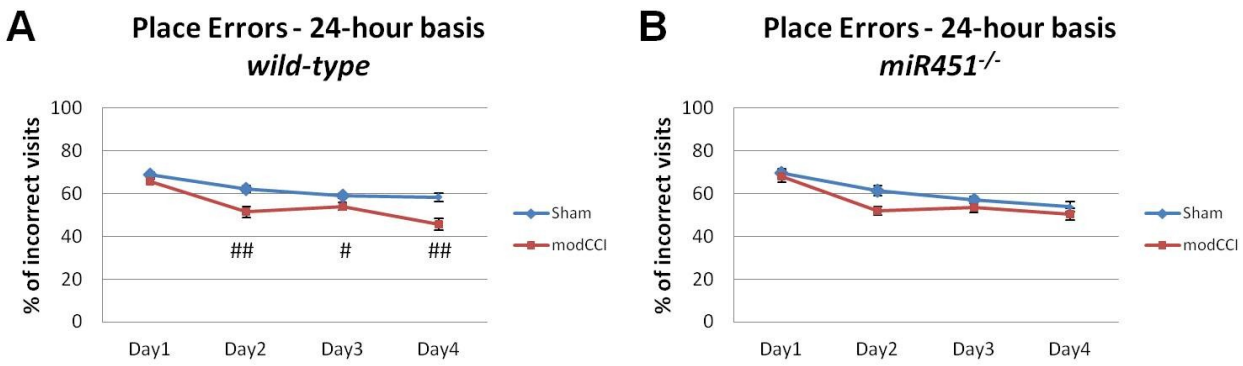

Figure 30: Learning performance of wild-type and miR451$^{-/-}$ mice at the Place Learning in IntelliCage

*The impact of the moderate CCI on the percentage of incorrect visits in the **A**) wild-type and **B**) miR451$^{-/-}$ mice was assessed in IntelliCage. In both groups statistically significant learning could be determined over time regardless of a brain trauma or sham surgery. But notably a significantly better learning performance was observed in the wild-type animals after moderate CCI compared to the respective sham controls, while the differences in miR451$^{-/-}$ groups did not reach statistical significance. Statistical significance of the observed differences was tested with mixed-model repeated measures ANOVA in the miR451$^{-/-}$ animals. In wild-type groups, however, repeated measures ANOVA (for time) and a one-way ANOVA (treatment) were used due to the significant Time X Treatment interaction. # p≤0.05, ## p≤0.01.*

In the wild-type animals a repeated measures ANOVA determined statistically significant learning in both sham ($F(3,24)=13.077$, $p<0.001$) and modCCI animals ($F(3,24)=16.494$, $p<0.001$) over the period of PL phase (*Figure 30* A). Differences between the treatment groups at each time point was assessed with one-way ANOVA and significant differences were observed at day 2 ($F(1,16)=12.381$, $p\leq0.01$), day 3 ($F(1,16)=6.420$, $p\leq0.05$) and day 4 post-TBI ($F(1,16)=13.270$, $p\leq0.01$) . It is noteworthy that these findings indicate a better learning performance in the trauma group at these days compared to the sham animals, in contradiction to an expected worsening in learning performance of traumatized animals.
In the miR451$^{-/-}$ animals, a similar learning was observed over the period of PL phase ($F(3,45)=36.213$, $p\leq0.001$) (*Figure 30* B). A slightly improved learning performance after TBI was observed with the miR451$^{-/-}$ animals similar to the wild-types, but the differences were not statistically significant ($F(1,15)=2.281$, $p=0.152$).

Next we analysed the place errors at the drink phases (2 hours, 00:00-01:00 and 05:00-06:00) and the place errors between the drink phases (01:00-05:00). The ratio of place errors at the interim to the place errors in the drink phases were taken as an indicator of short-term memory. Significantly higher ratios of *[place errors at the interim phase/place errors at the drink phase]* were observed in the trauma groups of both wild-type ($F(1,16)=9.892$, $p=0.006$) and miR451$^{-/-}$ animals ($F(1,15)=5.135$, $p=0.039$) were observed compared to the respective sham controls (*Figure 31* A, B).

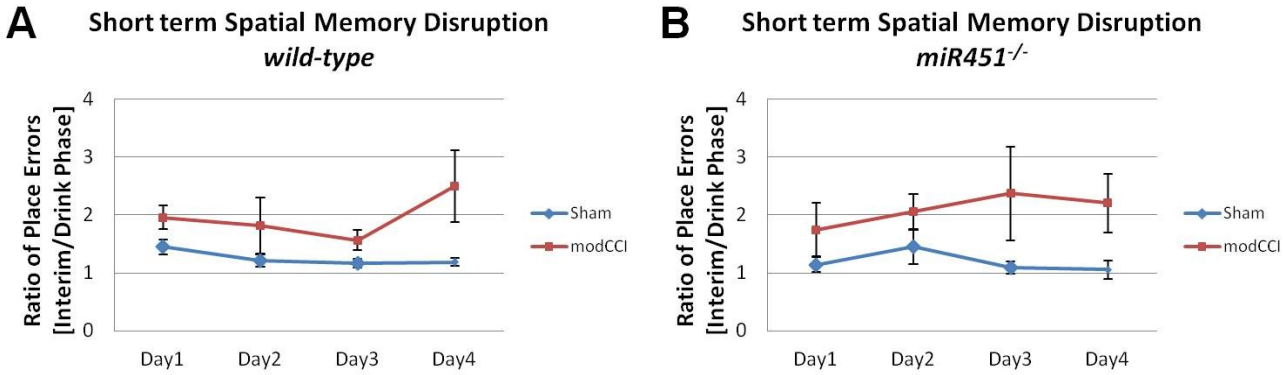

Figure 31: Short term memory performance in visit accuracy after moderate CCI in wild-type and miR451$^{-/-}$ animals.

*The impact of the moderate CCI on the short term memory performances as visit accuracy in **A**) wild-type and **B**) miR451$^{-/-}$ animals was assessed in the PL phase. In the trauma groups significantly higher ratios of* [place errors at the interim phase/place errors at the drink phase] *learning could be determined compared to the respective sham controls. Statistical significance of the observed differences was tested with mixed-model repeated measures ANOVA.*

When wild-type and miR451$^{-/-}$ animals were compared to each other separately for the treatment groups, mixed model repeated measure ANOVA tests did not determine any significant differences between the two genotypes in sham ($F(1,14)=0.857$, $p=0.370$) or modCCI animals ($F(1,17)=0.531$, $p=0.476$) in learning performance on a 24-hour basis. Similarly, the short-term memory performances (Ratio of *[place errors at the interim phase/place errors at the drink phase])* did not show any significant differences between the two genotypes in sham ($F(1,14)=0.288$, $p=0.600$) or modCCI animals ($F(1,17)=0.117$, $p=0.737$).

3.2.2 Nosepoke Errors

The analyses of the nosepoke activity were similar to the place errors.
When their activity was analysed on a 24-hour basis, differences were observed between nosepoke errors of the wild-type and miR451$^{-/-}$ animals after moderate TBI (*Figure 32*)

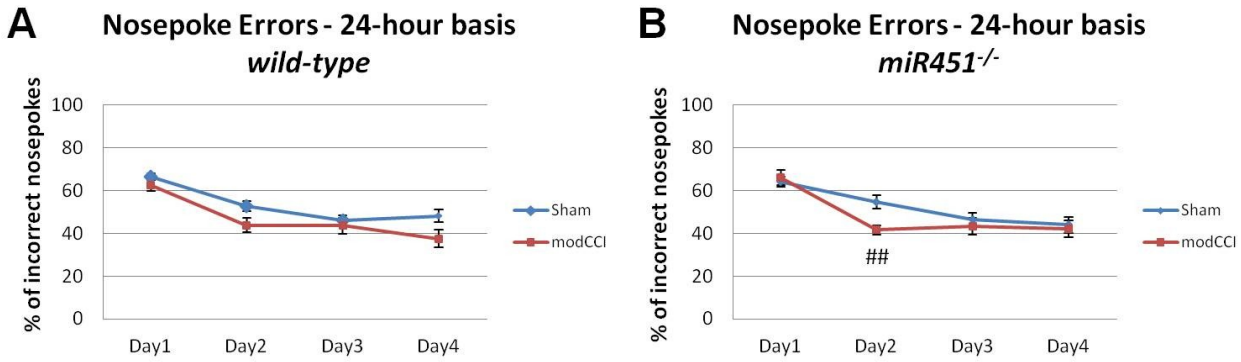

Figure 32: Nosepoke accuracy of wild-type and miR451$^{-/-}$ mice after moderate CCI or sham surgery.

*The impact of the moderate CCI on the nosepoke accuracy in **A**) wild-type and **B**) miR451$^{-/-}$ mice was assessed in the IntelliCage. In both groups statistically significant learning could be determined over time. The wild-type modCCI group showed not any statistically significant differences compared to the wild-type sham. However, significantly higher nosepoke accuracy was observed in the miR451$^{-/-}$ modCCI compared to the respective sham controls. Statistical significance of the observed differences (sham vs modCCI for each genotype) was tested with mixed-model repeated measures ANOVA in the wild-type animals. In miR451$^{-/-}$ groups, however, repeated measures ANOVA (for time) and a one-way ANOVA (for treatment) were used due to the significant Time X Treatment interaction. ## p≤0.01.*

Decreases in the nosepoke errors were observed in the wild-type animals regardless of the injury ($F(3,48)=36.392$, *p≤0.001*). Similar to the observation in the place errors, brain injured animals showed an improved performance in the nosepoke accuracy compared to the sham controls, but the differences did not reach to statistical significance ($F(1,16)=4.237$, *p=0.056*) (*Figure 32* A).
In the miR451$^{-/-}$ animals repeated measures ANOVA tests determined statistically significant learning in both sham ($F(3,18)=12.671$, *p<0.001*) and moderate CCI groups ($F(3,27)=27.760$, *p<0.001*) over the period of PL phase. Differences between the treatment groups at each time point was assessed with one-way

ANOVA and a significant difference was only observed at day 2 ($F(1,15)=12.189$, $p \leq 0.01$) (*Figure 32* B)

Next we analysed the nosepoke errors at the drink phases (2 hours, 00:00-01:00 and 05:00-06:00) and the nosepoke errors between the drink phases (01:00-05:00). Similar to the analyses conducted for the place errors in these phases, the ratio of nosepoke errors at the interim to the nosepoke errors in the drink phases were taken as an indicator of short-term memory. There was not any significantly different ratio of *[place errors at the interim phase/place errors at the drink phase]* observed in the trauma groups of either wild-type ($F(1,16)=2.558$, $p=0.129$) or miR451$^{-/-}$ animals ($F(1,15)=2.412$, $p=0.141$) compared to the respective sham controls (*Figure 33* A, B).

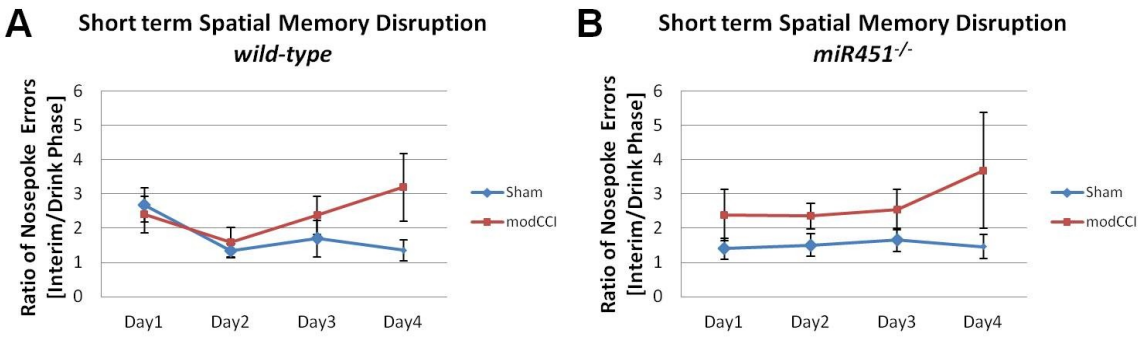

Figure 33: Short term memory performance in nosepoke accuracy after moderate CCI in wild-type and miR451$^{-/-}$ animals

*The impact of the moderate CCI on the short term memory performance as nosepoke accuracy in **A**) wild-type and **B**) miR451$^{-/-}$ mice was assessed in the PL phase. Although disturbances in short term memory performance was observed with the nosepoke accuracy in the injured animals, the differences were statistically not significant. Statistical significance of the observed differences was tested with mixed-model repeated measures ANOVA.*

When wild-type and miR451$^{-/-}$ animals were compared to each other separately for the treatment groups, mixed model repeated measure ANOVA tests did not determine any significant differences between the two genotypes in sham ($F(1,14)=0.187$, $p=0.672$) or modCCI animals ($F(1,17)=0.117$, $p=0.737$) in nosepoke errors on a 24-hour basis. Similarly, the short-term memory performances with respect to the nosepoke accuracy (Ratio of *[nosepoke errors at the interim phase/place errors at the drink phase])* did not show any significant differences between the two genotypes either in sham ($F(1,14)=0.750$, $p=0.401$) or moderate CCI groups ($F(1,17)=0.232$, $p=0.636$).

4 DISCUSSION

The involvement of miR451 in neuronal differentiation processes and as well as its presence in the CSF of TBI patients compared to non-injured controls has been described in literature (51,60). These recent findings lead to the attempt to evaluate the impact of miR451 on injury-induced neurogenesis in response to TBI in an experimental animal model.

In this study, we evaluated the impact of moderate TBI on adult neurogenesis in wild-type and miR451$^{-/-}$ mice. We analysed the numbers of BrdU+ and NeuN+ cells observed in hippocampi as well as the learning performance in a determined task testing spatial memory in the IntelliCage.

Histological analyses showed that the cell proliferation and neurogenesis were comparable between the wild-type and miR451$^{-/-}$ mice after a sham surgery. However, miR451$^{-/-}$ mice showed a much more pronounced cell proliferation and neurogenesis compared to the wild-type animals both in the ipsi- and contralateral dentate gyrus. Taken together, these data supported the hypothesis that the absence of miR451 in a trauma-associated environment would improve cell proliferation, differentiation and resilience of newly produced neurons. This finding correlates with the role of miR451 in human glioma cells, where it has been shown, that the miR451 inhibits cell growth and increased cell apoptosis (80,81), and the absence of miR451 contributes to the durability of newly proliferated neural cells in a pathophysiological microenvironment.

It should be noted that the increases in the post-TBI cell proliferation and neurogenesis was more pronounced in the contralateral regions. This could be explained by the particular susceptibility of newly produced neurons to the inflammatory microenvironment, which might hampered their survival till maturation (16).

As newly born neurons in the SGZ are excitatory cells (82,83), they migrate to the granular layer and are not expected to migrate to the hilus under physiological circumstances. Since the hilus allocates inhibitory neurons, the migration of new neurons from the SGZ into the hilus will also not compensate for the loss of inhibitory neurons following a brain injury. Instead, such aberrantly migrated excitatory cells in the hilus have been considered a characteristic observation in epileptic animal models (82,84–86) and as well have been reported to take place after brain injury, which at least partially explains the increased susceptibility to

epileptogenesis following a TBI (82,86,87). Although TBI-induced increases in neurogenesis is often thought to contribute to this aberrant migration (86,88), the actual molecular mechanism behind the phenomenon remained, so far, unclear. Nevertheless, the presence of higher number of newly produced neurons in the hilus might indicate an increased susceptibility of miR451$^{-/-}$ animals to develop *status epilepticus* following a traumatic brain injury. Whether this enhancement in aberrant migration of newly produced neurons from the SGZ to hilus is solely resulted from higher proliferation or whether miR451 has a regulatory role in neuronal migration require further studies to be elucidated.

Trauma-induced disturbances in the short-term spatial memory of wild-type and miR451$^{-/-}$ mice were assessed by analysing the visit or nosepoke errors during the "drink phase" and in between the "drink phases". The wild-type and miR451$^{-/-}$ brain injured animals differentiated from the sham controls with higher error rates as well as with a worsening in their error rates over time. These findings are in line with previous studies that show short-term memory deficiencies after TBI in experimental models (89). On the other hand, miR451 *per se* did not seem to play a role in the spatial memory performance in our settings, since the sham controls of wild type and miR451$^{-/-}$ mice performed comparably. Similarly, no significant differences were observed between the trauma groups of both genotypes. This suggests that the impact of newly produced neurons after brain trauma (enhanced in miR451$^{-/-}$ mice) on behavioural performance could rather be questionable, at least at the time period that we have chosen.

Interestingly, an improved spatial learning was observed in some modCCI groups in the 24-hour based analyses of learning performance (visit or nosepoke error rates) in the IntelliCage. It could be that the task composition used in the present study might be inadequate for detection of TBI-induced learning deficits at the analysed period of time (15-20 days post-TBI, place learning) between uninjured and CCI groups. In our cohorts, sham animals seemed to be performing a higher amount of random visits during the day, especially in the light phase, resulting in higher error rates compared to the injured animals. It seems that CCI animals were **i)** either less motivated to do random visits outside the drink phases due to emotional disturbances induced by TBI or **ii)** they were more motivated to access water and thereby paying more visits to the correct corner, due to excessive thirst. Indeed, there have been several studies reporting various social deficits in

experimental models of brain injury such as depression-like behaviour (90,91), which supports our first assumption. In addition to that, excessive thirst due to hypopituitarism is also well documented after clinical TBI (92), and a similar phenotype was shown in mice after CCI (93). Accordingly, we have observed a generally higher water consumption in the wild-type CCI group compared to the sham controls particularly in the first two days, supporting a contribution of TBI-induced hypopituitarism in better performance observed in this animal group. Taken together, it appears that our behavioural testing protocol to evaluate the learning performance was rather confounded by other post-traumatic morbidities, such as emotional disturbances and hypopituitarism, and thereby failed to distinguish between the actual learning performances in tested animal groups. Therefore, our findings indicate that standard task protocols widely used in IntelliCage in the literature are not very much suitable to assess the learning performance after traumatic brain injury. These findings, in fact, provided a strong basis for further establishment of IntelliCage protocols, tailored particularly for TBI animals in the future.

Finally, the impact of the newly produced neurons on the learning performance of the modCCI animals might not be covered in the time period presented in this study (day 15 after modCCI), as the maturation and functional integration of newly born neurons is reported to be completed at a later time point even under physiological conditions (33). The intended testing protocol in the present study takes 22 days, thereby the period between the place learning test and the sacrifice date was rather long (~25-30 days). It would be of particular interest in future experiments to allocate testing phase closer to the sample collection around 45 days. For that purpose, two options will be taken into consideration in the future: 1) planning shorter testing times (i.e. by excluding avoidance learning from the protocol) or 2) habituating the animals to the IntelliCage (including nosepoke learning) long before traumatic brain injury. Another option would be to do behavioural tests and histological analyses in separate animal cohorts at multiple time points, but this would require higher number of experimental animals and not preferable due to the ethical concerns.

Conclusion: All experimental groups had a significant decrease of the percentage of incorrect visits and nosepokes over time, indicating a learning progress.

In this study, no significant differences in learning abilities between the genotypes could be verified in direct comparisons of the sham or modCCI groups, which might be due to the time point of the analysed behavioural testing phase (15 days after trauma), where newly born neurons are not yet functionally integrated into the existing neuronal network.

The trend of modCCI groups performing better than sham controls could be caused by the absence of social rivalries in the injured animals, less motivation to do random visits due to emotional behavioural disturbances, or could be due to the excessive thirst caused by the TBI-induced hypopituitarism.

Concerning the proliferation and differentiation of cells in the hippocampus, the significant differences in sham to modCCI comparison where mainly seen in the contralateral hippocampus, suggesting that newly proliferated cells might rather survive in the contralateral side, than in the more injury-affected milieu of the ipsilateral hippocampus.

The miR451$^{-/-}$ comparison showed a significant increase of newly produced neurons exclusively in the contralateral dentate gyrus, while the wild-type modCCI group had no significant increase of newly produced neurons in the dentate gyrus. This leads to the conclusion that the absence of miR451 might improve the surviving of the susceptible newly proliferated neurons (80).

As a diploma thesis is limited concerning time and resources, it seems necessary to re-evaluate the impact of the miR451 in a CCI animal model, where perhaps a severe TBI group is included, or with further behavioural testing and the possibly with the investigation of post-traumatic epileptogenesis taken into account. It seems crucial, to evaluate the functional outcome at a later time-point after trauma. Finally a greater insight on the specific entity of the newly proliferated cells could be further investigated with additional histological, functional or electrophysiological methods.

5 BIBLIOGRAPHY

1. Faul, M., Xu, L., Wald, M. M. & Coronado VG. Traumatic brain injury in the United States: emergency department visits, hospitalizations and deaths 2002–2006. U.S. DEPARTMENT OF HEALTH AND HUMAN SERVICES Centers for Disease Control and Prevention National Center for Injury Prevention and Control. 2010.
2. Rutland-Brown W, Langlois J, Thomas K. Incidence of traumatic brain injury in the United States. J Head Trauma Rehabil. 2003;
3. Mauritz W, Brazinova A, Majdan M, Leitgeb J. Epidemiology of traumatic brain injury in Austria. Wien Klin Wochenschr. 2014;
4. Saatman KE, Duhaime A-C, Bullock R, Maas AIR, Valadka A, Manley GT. Classification of Traumatic Brain Injury for Targeted Therapies. J Neurotrauma. 2008;
5. Kaur P, Sharma S. Recent Advances in Pathophysiology of Traumatic Brain Injury. Curr Neuropharmacol. 2017;
6. Alluri H, Shaji CA, Davis ML, Tharakan B. A mouse controlled cortical impact model of traumatic brain injury for studying blood–brain barrier dysfunctions. In: Methods in Molecular Biology. 2018.
7. Corps KN, Roth TL, McGavern DB. Inflammation and neuroprotection in traumatic brain injury. JAMA Neurol. 2015;
8. Pan YB, Sun ZL, Feng DF. The Role of MicroRNA in Traumatic Brain Injury. Neuroscience. 2017.
9. Wang X, Gao X, Michalski S, Zhao S, Chen J. Traumatic Brain Injury Severity Affects Neurogenesis in Adult Mouse Hippocampus. J Neurotrauma. 2015;
10. Gao X, Chen J. Moderate traumatic brain injury promotes neural precursor proliferation without increasing neurogenesis in the adult hippocampus. Exp Neurol. 2013;
11. Chirumamilla S, Sun D, Bullock MR, Colello RJ. Traumatic brain injury induced cell proliferation in the adult mammalian central nervous system. J Neurotrauma. 2002;
12. Kernie SG, Erwin TM, Parada LF. Brain remodeling due to neuronal and astrocytic proliferation after controlled cortical injury in mice. J Neurosci Res. 2001;

13. Rice AC, Khaldi A, Harvey HB, Salman NJ, White F, Fillmore H, et al. Proliferation and neuronal differentiation of mitotically active cells following traumatic brain injury. Exp Neurol. 2003;
14. Rola R, Mizumatsu S, Otsuka S, Morhardt DR, Noble-Haeusslein LJ, Fishman K, et al. Alterations in hippocampal neurogenesis following traumatic brain injury in mice. Exp Neurol. 2006;
15. Dixon CE, Kochanek PM, Yan HQ, Schiding JK, Griffith RG, Baum E, et al. One-year study of spatial memory performance, brain morphology, and cholinergic markers after moderate controlled cortical impact in rats. J Neurotrauma. 1999;
16. Gao X, Deng-Bryant Y, Cho W, Carrico KM, Hall ED, Chen J. Selective death of newborn neurons in hippocampal dentate gyrus following moderate experimental traumatic brain injury. J Neurosci Res. 2008;
17. Daniel L.HausabLuciLópez-VelázquezdEric M.GoldabKelly M.CunninghamdHarveyPerezdAileen J.AndersonabcdBrian J.Cummingsabcd. Transplantation of human neural stem cells restores cognition in an immunodeficient rodent model of traumatic brain injury. Exp Neurol [Internet]. 2016 Jul 1 [cited 2017 Oct 11];281:1–16. Available from: http://han.medunigraz.at/han/rio/www.sciencedirect.com/science/article/pii/S0014488616300887
18. Romine J, Gao X, Chen J. Controlled Cortical Impact Model for Traumatic Brain Injury. 2014;(August):13–6.
19. Osier ND, Dixon CE. The controlled cortical impact model: Applications, considerations for researchers, and future directions. Frontiers in Neurology. 2016.
20. Altman J. Are new neurons formed in the brains of adult mammals? Science (80-). 1962;
21. Altman J, Das GD. Autoradiographic and histological evidence of postnatal hippocampal neurogenesis in rats. J Comp Neurol. 1965;
22. Eriksson PS, Perfilieva E, Björk-Eriksson T, Alborn AM, Nordborg C, Peterson DA, et al. Neurogenesis in the adult human hippocampus. Nat Med. 1998;
23. Kempermann, MD G, Kempermann, MD G. Adult Hippocampal Neurogenesis. In: Adult Neurogenesis 2. 2013.

24. Gage FH. Mammalian neural stem cells. Science. 2000.
25. Gould E, Tanapat P, McEwen BS, Flügge G, Fuchs E. Proliferation of granule cell precursors in the dentate gyrus of. Proceedings of the National Academy of Sciences. 1998.
26. Ming G li, Song H. Adult Neurogenesis in the Mammalian Brain: Significant Answers and Significant Questions. Neuron. 2011.
27. Doetsch F, Alvarez-Buylla A. Network of tangential pathways for neuronal migration in adult mammalian brain. Proc Natl Acad Sci. 2002;
28. Cameron HA, Woolley CS, McEwen BS, Gould E. Differentiation of newly born neurons and glia in the dentate gyrus of the adult rat. Neuroscience. 1993;
29. Ohira K. Injury-induced neurogenesis in the mammalian forebrain. 2011;1645–56.
30. Vishwakarma SK, Bardia A, Tiwari SK, Paspala SAB, Khan AA. Current concept in neural regeneration research: NSCs isolation, characterization and transplantation in various neurodegenerative diseases and stroke: A review. Journal of Advanced Research. 2014.
31. Li L, Xie T. STEM CELL NICHE: Structure and Function. Annu Rev Cell Dev Biol. 2005;
32. Steiner B, Klempin F, Wang L, Kott M, Kettenmann H, Kempermann G. Type-2 cells as link between glial and neuronal lineage in adult hippocampal neurogenesis. Glia. 2006;
33. Kempermann G, Jessberger S, Steiner B, Kronenberg G. Milestones of neuronal development in the adult hippocampus. Trends Neurosci. 2004;
34. Deng W, Aimone JB, Gage FH. New neurons and new memories: How does adult hippocampal neurogenesis affect learning and memory? Nature Reviews Neuroscience. 2010.
35. Parent JM. Neuroscientist Injury-Induced Neurogenesis in the Adult Mammalian Brain. 2003;
36. Ngwenya LB, Danzer SC. Impact of traumatic brain injury on neurogenesis. Front Neurosci. 2019;
37. Lee RC, Feinbaum RL, Ambros V. The C. elegans heterochronic gene lin-4 encodes small RNAs with antisense complementarity to lin-14. Cell. 1993;
38. Bartel DP. MicroRNAs: Genomics, Biogenesis, Mechanism, and Function.

Cell. 2004.
39. Griffiths-Jones S, Saini HK, Van Dongen S, Enright AJ. Griffithsjones S, Saini H K, Dongen S V, et al. miRBase: tools for microRNA genomics[J]. Nucleic Acids Research, 2008, 36: 154-8. Nucleic Acids Res. 2008;
40. Kozomara A, Griffiths-Jones S. MiRBase: Annotating high confidence microRNAs using deep sequencing data. Nucleic Acids Res. 2014;
41. Lang MF, Shi Y. Dynamic roles of microRNAs in neurogenesis. Front Neurosci. 2012;
42. Stappert L, Roese-Koerner B, Brüstle O. The role of microRNAs in human neural stem cells, neuronal differentiation and subtype specification. Cell and Tissue Research. 2015.
43. R. S, G.M. S. MicroRNAs in neuronal development, function and dysfunction. Brain Res. 2010;
44. Smirnova L, Gräfe A, Seiler A, Schumacher S, Nitsch R, Wulczyn FG. Regulation of miRNA expression during neural cell specification. Eur J Neurosci. 2005;
45. Silber J, Lim DA, Petritsch C, Persson AI, Maunakea AK, Yu M, et al. miR-124 and miR-137 inhibit proliferation of glioblastoma multiforme cells and induce differentiation of brain tumor stem cells. BMC Med. 2008;
46. Edbauer D, Neilson JR, Foster KA, Wang CF, Seeburg DP, Batterton MN, et al. Regulation of Synaptic Structure and Function by FMRP-Associated MicroRNAs miR-125b and miR-132. Neuron. 2010;
47. Szulwach KE, Li X, Smrt RD, Li Y, Luo Y, Lin L, et al. Cross talk between microRNA and epigenetic regulation in adult neurogenesis. J Cell Biol. 2010;
48. Siegel G, Obernosterer G, Fiore R, Oehmen M, Bicker S, Christensen M, et al. A functional screen implicates microRNA-138-dependent regulation of the depalmitoylation enzyme APT1 in dendritic spine morphogenesis. Nat Cell Biol. 2009;
49. Liu C, Teng ZQ, Santistevan NJ, Szulwach KE, Guo W, Jin P, et al. Epigenetic regulation of miR-184 by MBD1 governs neural stem cell proliferation and differentiation. Cell Stem Cell. 2010;
50. Liu C, Teng ZQ, McQuate AL, Jobe EM, Christ CC, von Hoyningen-Huene SJ, et al. An Epigenetic Feedback Regulatory Loop Involving MicroRNA-195 and MBD1 Governs Neural Stem Cell Differentiation. PLoS One. 2013;

51. Trattnig C, Üçal M, Tam-Amersdorfer C, Bucko A, Zefferer U, Grünbacher G, et al. MicroRNA-451a overexpression induces accelerated neuronal differentiation of Ntera2/D1 cells and ablation affects neurogenesis in microRNA-451a -/- mice. PLoS One. 2018;
52. Sun E, Shi Y. MicroRNAs: Small molecules with big roles in neurodevelopment and diseases. Experimental Neurology. 2015.
53. Zhan M, Miller CP, Papayannopoulou T, Stamatoyannopoulos G, Song CZ. MicroRNA expression dynamics during murine and human erythroid differentiation. Exp Hematol. 2007;
54. Bian HB, Pan X, Yang JS, Wang ZX, De W. Upregulation of microRNA-451 increases cisplatin sensitivity of non-small cell lung cancer cell line (A549). J Exp Clin Cancer Res. 2011;
55. Wang R, Wang ZX, Yang JS, Pan X, De W, Chen LB. MicroRNA-451 functions as a tumor suppressor in human non-small cell lung cancer by targeting ras-related protein 14 (RAB14). Oncogene. 2011;
56. Bandres E, Bitarte N, Arias F, Agorreta J, Fortes P, Agirre X, et al. microRNA-451 regulates macrophage migration inhibitory factor production and proliferation of gastrointestinal cancer cells. Clin Cancer Res. 2009;
57. Yuan J, Lang J, Liu C, Zhou K, Chen L, Liu Y. The expression and function of miRNA-451 in osteosarcoma. Med Oncol. 2015;
58. Pan X, Wang R, Wang Z-X. The Potential Role of miR-451 in Cancer Diagnosis, Prognosis, and Therapy. Mol Cancer Ther. 2013;
59. Godlewski J, Nowicki MO, Bronisz A, Nuovo G, Palatini J, De Lay M, et al. MicroRNA-451 Regulates LKB1/AMPK Signaling and Allows Adaptation to Metabolic Stress in Glioma Cells. Mol Cell. 2010;
60. Patz S, Trattnig C, Grünbacher G, Ebner B, Gülly C, Novak A, et al. More than Cell Dust: Microparticles Isolated from Cerebrospinal Fluid of Brain Injured Patients Are Messengers Carrying mRNAs, miRNAs, and Proteins. J Neurotrauma. 2013;
61. Calderone L, Grimes P, Shalev M. Acute reversible cataract induced by xylazine and by ketamine-xylazine anesthesia in rats and mice. Exp Eye Res. 1986;42(4):331–7.
62. Corne R, Leconte C, Ouradou M, Fassina V, Zhu Y, Déou E, et al. Spontaneous resurgence of conditioned fear weeks after successful

extinction in brain injured mice. Prog Neuro-Psychopharmacology Biol Psychiatry. 2019;

63. Cho C, Michalidis V, Lecker I, Collymore C, Hanwell D, Loka M, et al. Evaluating analgesic efficacy and administration route following craniotomy in mice using the grimace scale. Sci Rep. 2019;
64. Kawai T, Takagi N, Miyake-Takagi K, Okuyama N, Mochizuki N, Takeo S. Characterization of BrdU-Positive Neurons Induced by Transient Global Ischemia in Adult Hippocampus. J Cereb Blood Flow Metab. 2004;
65. Galsworthy MJ, Amrein I, Kuptsov PA, Poletaeva II, Zinn P, Rau A, et al. A comparison of wild-caught wood mice and bank voles in the Intellicage: Assessing exploration, daily activity patterns and place learning paradigms. Behav Brain Res. 2005;157(2):211–7.
66. Mechan AO, Wyss A, Rieger H, Mohajeri MH. A comparison of learning and memory characteristics of young and middle-aged wild-type mice in the IntelliCage. J Neurosci Methods [Internet]. 2009;180(1):43–51. Available from: http://dx.doi.org/10.1016/j.jneumeth.2009.02.018
67. Codita A, Gumucio A, Lannfelt L, Gellerfors P, Winblad B, Mohammed AH, et al. Impaired behavior of female tg-ArcSwe APP mice in the IntelliCage: A longitudinal study. Behav Brain Res [Internet]. 2010;215(1):83–94. Available from: http://dx.doi.org/10.1016/j.bbr.2010.06.034
68. Barlind A, Karlsson N, Björk-Eriksson T, Isgaard J, Blomgren K. Decreased cytogenesis in the granule cell layer of the hippocampus and impaired place learning after irradiation of the young mouse brain evaluated using the IntelliCage platform. Exp Brain Res. 2010;201(4):781–7.
69. Jaholkowski P, Kiryk A, Jedynak P, Ben Abdallah NM, Knapska E, Kowalczyk A, et al. New hippocampal neurons are not obligatory for memory formation; cyclin D2 knockout mice with no adult brain neurogenesis show learning. Learn Mem [Internet]. 2009;16(7):439–51. Available from: http://learnmem.cshlp.org/cgi/doi/10.1101/lm.1459709
70. Gage GJ, Kipke DR, Shain W. Whole Animal Perfusion Fixation for Rodents. J Vis Exp. 2012;
71. Tremblay M-É, Riad M, Majewska A. Preparation of Mouse Brain Tissue for Immunoelectron Microscopy. J Vis Exp. 2010;
72. Wojtowicz JM, Kee N. BrdU assay for neurogenesis in rodents. Nat Protoc.

2006;
73. Gould E, Tanapat P, McEwen BS, Flugge G, Fuchs E. Proliferation of granule cell precursors in the dentate gyrus of adult monkeys is diminished by stress. Proc Natl Acad Sci. 2002;
74. Leuner B, Glasper ER, Gould E. Thymidine analog methods for studies of adult neurogenesis are not equally sensitive. J Comp Neurol. 2009;
75. Mullen RJ, Buck CR, Smith AM. NeuN, a neuronal specific nuclear protein in vertebrates. Development. 1992;
76. Dent MAR, Segura-Anaya E, Alva-Medina J, Aranda-Anzaldo A. NeuN/Fox-3 is an intrinsic component of the neuronal nuclear matrix. FEBS Lett. 2010;
77. Verdiev BI, Poltavtseva RA, Podgornyi O V., Marei M V., Zinovyeva RD, Sukhikh GT, et al. Molecular genetic and immunophenotypical analysis of PaX6 transcription factor and neural differentiation markers in human fetal neocortex and retina in vivo and in vitro. Bull Exp Biol Med. 2009;
78. Wolf HK, Buslei R, Schmidt-Kastner R, Schmidt-Kastner PK, Pietsch T, Wiestler OD, et al. NeuN: A useful neuronal marker for diagnostic histopathology. J Histochem Cytochem. 1996;
79. Weyer A, Schilling K. Developmental and cell type-specific expression of the neuronal marker NeuN in the murine cerebellum. J Neurosci Res. 2003;
80. Nan Y, Han L, Zhang A, Wang G, Jia Z, Yang Y, et al. MiRNA-451 plays a role as tumor suppressor in human glioma cells. Brain Res. 2010;
81. Ogawa D, Ansari K, Nowicki MO, Salińska E, Bronisz A, Godlewski J. MicroRNA-451 inhibits migration of glioblastoma while making it more susceptible to conventional therapy. Non-coding RNA. 2019;
82. Hunt RF, Scheff SW, Smith BN. Posttraumatic epilepsy after controlled cortical impact injury in mice. Exp Neurol. 2009;
83. Lazarov O, Hollands C. Hippocampal neurogenesis: Learning to remember. Progress in Neurobiology. 2016.
84. Hunt RF, Boychuk JA, Smith BN. Neural circuit mechanisms of posttraumatic epilepsy. Frontiers in Cellular Neuroscience. 2013.
85. Kelly KM, Miller ER, Lepsveridze E, Kharlamov EA, Mchedlishvili Z. Posttraumatic seizures and epilepsy in adult rats after controlled cortical impact. Epilepsy Res. 2015;
86. Neuberger EJ, Swietek B, Corrubia L, Prasanna A, Santhakumar V.

Enhanced Dentate Neurogenesis after Brain Injury Undermines Long-Term Neurogenic Potential and Promotes Seizure Susceptibility. Stem Cell Reports. 2017;

87. Hunt RF, Scheff SW, Smith BN. Regionally localized recurrent excitation in the dentate gyrus of a cortical contusion model of posttraumatic epilepsy. J Neurophysiol. 2010;
88. Ibrahim S, Hu W, Wang X, Gao X, He C, Chen J. Traumatic Brain Injury Causes Aberrant Migration of Adult-Born Neurons in the Hippocampus. Sci Rep. 2016;
89. Park M-S, Oh H-A, Ko I-G, Kim S-E, Kim S-H, Kim C-J, et al. Influence of mild traumatic brain injury during pediatric stage on short-term memory and hippocampal apoptosis in adult rats. J Exerc Rehabil. 2014;
90. Pandey DK, Yadav SK, Mahesh R, Rajkumar R. Depression-like and anxiety-like behavioural aftermaths of impact accelerated traumatic brain injury in rats: A model of comorbid depression and anxiety? Behav Brain Res. 2009;
91. Bondi CO, Semple BD, Noble-Haeusslein LJ, Osier ND, Carlson SW, Dixon CE, et al. Found in translation: Understanding the biology and behavior of experimental traumatic brain injury. Neuroscience and Biobehavioral Reviews. 2015.
92. Klose M, Feldt-Rasmussen U. Hypopituitarism in Traumatic Brain Injury—A Critical Note. J Clin Med. 2015;
93. Osterstock G, Yandouzi T El, Romanò N, Carmignac D, Langlet F, Coutry N, et al. Sustained alterations of hypothalamic tanycytes during posttraumatic hypopituitarism in male mice. Endocrinology. 2014;

6 APPENDIX

6.1 Animals

Wild-type sham group:

The average age of animals of the wild-type sham group was 14 weeks. The average weight on the day of the surgery was 24.22 g and on day 45 after trauma, the average weight was 24.78 g. Therefore the average weight difference was 0.56 g.

Table 1

Number	Age at Day 0	weight at Day 0	Weight at day 45	Complications
0153-0171	14	24	25	
0153-0173	14	23	24	
0153-0175	14	24	24	
0153-0177	14	25	25	
0153-3485	14	25	26	
0153-3487	14	26	25	
0153-3489	14	24	25	
0153-3491	14	23	25	
0153-3493	14	24	24	
0153-0169	14	25	27	

Wild-type CCI group:

Animals in the wild-type modCCI group had an average age of 14 weeks and an average weight of 25.45 g at the day of the moderate trauma. At day 45, the average weight of the animal was 25.73 g, resulting in an average gain of weight of 0.27g.

Table 2

Number	Age at Day 0	weight at Day 0	Weight at day 45	Complications
0153-3553	14	24	26	
0153-3555	14	26	26	
0153-3557	14	26	26	dehydration - excluded
0153-3559	14	27	25	dehydration - excluded
0153-3561	14	24	24	
0153-3563	14	26	26	
0153-3565	14	25	25	
0153-3567	14	25	26	
0153-3569	14	25	25	
0153-3571	14	27	27	

Animals 0153-3557 and 0153-3559 had to be excluded due to dehydration caused by non- learning of the nosepoke principle, to gain access to the water bottles during the nosepoke phase. They were taken out of the IntelliCage on day 10 after trauma and were housed in a conventional cage until day 45.

miR451 $^{-/-}$ sham group:

In the miR451$^{-/-}$ sham group, the average age at the day of the surgery was 10.5 weeks. The average weight at the day of the surgery was 24.63 g and 26.00 g at day 45 after surgery, resulting in an average weight gain of 1.38 g, per animal.

Table 3

Number	Age at Day 0	weight at Day 0	Weight at Day 45	Complications
5092-0975	10	26	26	RFID chip removed
5092-0987	10	27	28	dehydration – excluded
5092-0989	10	26	27	
5092-0991	10	25	26	
5092-0993	11	23	26	
5092-0995	11	23	25	
5092-0997	11	23	24	
5092-0999	11	24	26	

Animal 5092-0975 removed the RFID chip on day 6 and had to be re-chipped on day 7 during the anaesthesia BrdU injections.
Animal 5092-0987 had to be excluded from further behavioural testing, because it could not achieve to nosepoke in order to get access to the water bottles. After 24 hours of water restriction (not enough licks registered by the IntelliCage), the animal was taken out of the IntelliCage and housed in a conventional cage with free access to water until day 45.

miR451 $^{-/-}$ CCI group:
In the miR451$^{-/-}$ moderate CCI group, the average age of the animals was approximately 12.5 weeks. On the day of the moderate trauma, the average weight of the animals was 24.9 g and 26.2 g on day 45 after trauma. The average weight gain per mouse was 1.3 g.

Table 4

Number	Age at Day 0	Weight at Day 0	Weight at day 45	Complications
5092-1001	13	26	28	
5092-1003	13	25	26	wound dehiscence
5092-1005	13	27	27	
5092-1007	13	24	26	RFID chip removed
5092-1009	13	26	26	
5092-1011	13	24	25	
5092-1013	13	25	27	
5092-1015	13	25	26	
5092-1017	12	23	25	
5092-1019	12	24	26	

Animal 5092-1003 developed a wound dehiscence which had to be closed on day 7 with a secondary single knot suture, while the animal was still anesthetized because of the BrdU injection.
Animal 5092-1007 removed the implanted RFID chip on day 7 and had to be re chipped with a new RFID chip during the BrdU injection (under isoflurane anaesthesia) the same day.